Enhancement of Noisy Planar Nuclear Medicine Images using Mean Field Annealing

Daniyel Lennard Falk

A dissertation submitted to the Faculty of Engineering and the Built Environment, University of the Witwatersrand, Johannesburg, in fulfilment of the requirements for the degree of Master of Science in Engineering.

Johannesburg, October 2007

Declaration

I declare that this dissertation is my own, unaided work, except where otherwise acknowledged. It is being submitted for the degree of Master of Science in Engineering to the University of the Witwatersrand, Johannesburg. It has not been submitted before for any degree or examination in any other university.

The use of clinical images in this study was approved by the Human Research Ethics Committee of the University of the Witwatersrand, Johannesburg (protocol no. M060312).

Signed this ___ day of _____ 20___

_____

Daniyel Lennard Falk.

Abstract

Nuclear Medicine (NM) images inherently suffer from large amounts of noise and blur. The purpose of this research is to reduce the noise and blur while maintaining image integrity for improved diagnosis. The proposal is to further improve image quality after the standard pre- and post-processing undertaken by a gamma camera system.

Mean Field Annealing (MFA), the image processing technique used in this research is a well known image processing approach. The MFA algorithm uses two techniques to achieve image restoration. Gradient descent is used as the minimisation technique, while a deterministic approximation to Simulated Annealing (SA) is used for optimisation. The algorithm anisotropically diffuses an image, iteratively smoothing regions that are considered non-edges and still preserving edge integrity until a global minimum is obtained. A known advantage of MFA is that it is able to minimise to this global minimum, skipping over local minima while still providing comparable results to SA with significantly less computational effort.

Image blur is measured using either a point or line source. Both allow for the derivation of a Point Spread Function (PSF) that is used to de-blur the image. The noise variance can be measured using a flood source. The noise is due to the random fluctuations in the environment as well as other contributors. Noisy blurred NM images can be difficult to diagnose particularly at regions with steep intensity gradients and for this reason MFA is considered suitable for image restoration.

From the literature it is evident that MFA can be applied successfully to digital phantom images providing improved performance over Wiener filters. In this paper MFA is shown to yield image enhancement of planar NM images by implementing a sharpening filter as a post MFA processing technique.

To JP, I will never forget you!

Acknowledgements

I would like to thank:

- My supervisor Professor D. Rubin for all his supreme effort, insight and guidance that brought this work to fruition.
- My co-supervisor Professor T. Marwala, for his input and advice.
- Professor Vangu of the Department of Nuclear Medicine at Wits University for providing the research facilities required in this study.
- From the Medical Physics Department, Mr. Sibusiso Jozela for his time spent acquiring the experimental data and Mr. Nico van der Merwe for his input.
- Professor A. van Rensburg from Medical Physics at the University of Pretoria, for his useful suggestions on imaging line sources.
- Dr. Cindy Perumal for her time spent explaining Nuclear Medicine to an engineer.
- In particular I would like to thank my parents for their unwavering conviction, exceptional support and sturdy advice.
- My family and friends who have unbroken faith in me.
- The staff in the school of Electrical and Information Engineering for their help and advice.
- My fellow post-grads at Wits for their wit and valuable suggestions, particularly D. Starfield and L. Joffe.

Contents

List of Figures

Nomenclature

Acronym	Meaning
ASA	Adaptive Simulated Annealing
BAD	Biased Anisotropic Diffusion
BFGS	Broyden-Fletcher-Goldfarb-Shannon
CT	Computered Tomography
DOG	Difference Of Gaussian
FWHM	Full Width at Half Maximum
GE	General Electric
GNC	Graduated Non-Convexity
GUI	Graphical User Interface
LOG	Laplacian Of Gaussian
LSF	Line Spread Function
MAP	Maximum A-posteriori Problem
MFA	Mean Field Annealing
MFT	Mean Field Theory
ML	Maximum Likelihood
MRF	Markov Random Field
MRI	Magnetic Resonance Imaging
MTF	Modulation Transfer Function
NM	Nuclear Medicine
PET	Positron Emission Tomography
PM	Photo-Multiplier
PSF	Point Spread Function
PSNR	Peak Signal to Noise Ratio
RMSE	Root Mean Square Error
ROC	Receiver Operating Characteristic
SA	Simulated Annealing
SPECT	Single Photon Emission Computed Tomography
VCD	Variable Conductance Diffusion
VFSR	Very Fast Simulated Reannealing

Chapter 1

Introduction

Medical imaging techniques began with X-rays that were discovered by *W.C. Röntgen* in 1895 and soon thereafter the prospect of medical diagnosis was recognized [1]. There are now many different imaging techniques accessible to the medical community; notably these include Radiology and Computered Tomography (CT) with X-rays, Diagnostic Ultrasound, Nuclear Magnetic Resonance Imaging (MRI), Electrical Impedance Tomography and Radioisotope Imaging. This research is focused on Radioisotope Imaging and its derivatives.

In Radioisotope Imaging (planar Nuclear Medicine (NM) imaging) the radiation originates from inside the body and this is fundamentally different from the other imaging techniques. Radioisotope-tagged compounds in tracer quantities (known as a radiotracer or radiopharmaceutical) are injected into the patient's body where the isotopes decay and produce gamma-photons. These γ-photons are detectable and therefore it is possible to obtain images of the distribution of the radionuclide. Depending on the choice of labeling agent, the distribution of radionuclide can be representative of different physiological functions, such as blood flow, blood volume or various metabolic processes.

The processes and physics of Radioisotope Imaging has been well established with progressively advancing techniques appearing such as Single Photon Emission Computed Tomography (SPECT) and Positron Emission Tomography (PET). However, due to the physical constraints of both γ-photon detection techniques and the restricted amounts of radiotraces that may be administered, the resolution of Radioisotope Imaging is limited. As a result, the image quality sub-standard when compared to anatomical medical images such as MRI and CT scans. The purpose of this dissertation is to investigate the use of the computational technique Mean

Field Annealing (MFA) and other post processing filters to improve the overall image quality of Radioisotope images.

MFA is an iterative computational technique that makes use of the Point Spread Function (PSF) and the noise associated with the NM image. MFA is applied to NM images with the objective of reducing noise without compromising edge integrity. Furthermore, using a sharpening filter as a post-MFA technique may yield subjective image enhancement of planar NM images.

1.1 Progression of Dissertation

This dissertation has been structured to provide a technical understanding of how MFA can be applied to NM images. A technical paper discussing this application has been published [2].

Chapter 2 introduces a basic description and background of Nuclear Medicine Imaging details and some diagnosic issues.

Chapter 3 describes general image restoration techniques focusing in detail on the importance of the accuracy of data models in order to achieve a successful image restoration result. The prior knowledge required is the determination of an accurate Point Spread Function and noise data model.

Chapter 4 describes and reviews Mean Field Annealing beginning with a brief discussion of the origins of MFA. It then continues with a mathematically comprehensive review of the derivation of MFA based on a Bayesian approach. The Chapter also details different techniques available in edge detection and optimisation required in MFA. In addition it describes the MFA algorithm as an iterative technique.

Chapter 5 addresses the application of MFA to digital phantom images as a proof of concept. This chapter focuses on parameter selection, stopping criteria and digital phantom restoration results.

Chapter 6 discusses how MFA can be applied to NM images highlighting the problems and requirements surrounding implementation. It also addresses the results of MFA applied to NM images from an image reconstruction point of view.

Chapter 7 summarises and concludes the study and lists all the recommendations by the author for future work in MFA applied to Nuclear Medicine

Chapter 2

Review of Nuclear Medicine Imaging

Numerous factors affect how a scan is performed and these factors will in turn influence the quality and characteristics of the images. Different types of NM images require different exposure durations and delays between injection and scanning. For instance a bone scan requires 2-4 hours before scanning can begin while other scans only require delays of a couple of minutes. The distance of the collimator to the target organ and attenuation from other organs and tissues are two examples that may affect image intensity and quality. The total distance the γ-photons need to travel is a function of both target organ depth as well collimator distance away from the body. This distance affects the variance of the Gaussian distribution associated with the blur that is fundamental to the image restoration process used in this study.

Currently the NM cameras available typically have software that can threshold, invert, non-linearly scale, eliminate background and perform other standard image processing functionality. Regardless, edges are not enhanced to the standards of anatomical imagery (CT, MRI etc.).

There are many issues that need to be factored in when diagnosing using NM images. Some of these factors are outlined below:

- Overlying bones tend to look more intense but this could be because the radiation is radiating from two overlapping bones, and does not always imply a region of high uptake.
- Background activity is not necessarily noise, i.e. small amounts of the radiotracer may actually be in those regions interspersed with the noise. NM physicians determine the difference between noise and background activity by anticipating a certain distribution.

- Star effects are artifacts that typically occur with high energy radiopharmaceuticals such as Iodine that goes directly to the thyroid.

- Clinicians are often interested in both hot and cold regions. Hot implies regions of high uptake and cold being regions where there is reduced uptake. It is often difficult to identify the cold regions due to the influence of noise. Sometimes the simple solution of inverting the image can help solve this problem.

- Vertebrae and other bone detail are frequently not sufficiently defined in bone scans (skeletal). For example in a patient suffering from scoliosis the higher vertebra are often not as well defined as the lower vertebra.

- Infection may require the use of Gallium, however this results in poor quality images. It is imperative to see where the Gallium has been taken up but Gallium has a higher energy and penetrates through the septae of a collimator. Generally lower energy radiopharmaceuticals provide a more estimable quality image even though intrinsic resolution becomes worse with decreasing gamma ray energy [3]. Due to diagnostic difficulty another type of scan may be introduced to reinforce the results. Often multiple views are required in the diagnostic process.

Chapter 3

Image Restoration

There are many different strategies when it comes to image restoration such as non-linear extrapolation in frequency space [4], Wiener filters [5], median filters, weighted median filters, average filters, Graduated Non-Convexity (GNC), Variable Conductance Diffusion (VCD), Anisotropic Diffusion and Biased Anisotropic Diffusion (BAD) [6] and many more. Different techniques are suitable for different types of images, and often the correct combination of techniques will yield the best results. Mean Field Annealing is another technique that has been shown to be qualitatively equivalent to GNC [7] and is the primary technique that will be investigated in this study. The following chapter will discuss the prerequisites for MFA.

3.1 General

All images are imperfect and can be described as reflecting the scene as well as the quality of the imaging system. Images can be degraded in the following ways.

- Image distortion due to the point spread function associated with the particular imaging system.
- Random noise added to the image due to the environment.
- Random noise added to the image due to the imaging systems (electronic noise etc).

Consider a recorded image g and an ideal (non-degraded) image f of a scene. The recorded image is a function of the distortion D and the combined total noise n.

$$g = Df + n \tag{3.1}$$

Image restoration aims to reverse the impact of D and n in Equation 3.1. This requires some knowledge of how the image has been blurred and affected by the statistical noise.

3.2 Point Spread Function

There are many parameters that define how well a gamma camera performs, these parameters include:

- Sharpness and detail (spatial resolution).
- The efficiency with which it detects incident radiation.
- Ability to measure the energy in incident γ-rays i.e. minimise scatter.
- Counting rate it can handle without significant dead-time losses.

In reality a gamma camera is not able to produce ideal images of the radionuclide distribution. Its imperfections are caused by performance characteristics of the detector, associated electronic circuitry and the collimator. Malfunctions in various camera components can also cause image artifacts [3]. Therefore standard tests and calibrations are frequently performed on γ-cameras. Important information such as the Point Spread Function (PSF) or Modulation Transfer Function (MTF) needs to be obtained to keep the cameras operating correctly.

There are many aspects that contribute to the overall spatial resolution of the image such as intrinsic spatial resolution and energy resolution (for further details see *Physics in Nuclear Medicine* [3]). The resolution of the collimator is a major factor in determining the overall resolution of the NM images.

Other detector limitations include nonlinearity and non-uniformity. Nonlinearities arise when there is a nonlinear change of X and Y signals with the displacement distance of a radiation source (occurring across the surface of the detector) [3]. This can

result in pincushion distortion and barrel distortion. Pincushion distortion events are pushed toward the center of the distortion and barrel distortions are pushed outward causing hot spots and cold spots respectively [3]. With todays electronic technology these distortions can be easily countered, however they can have significant effects on image non-uniformities.

Non-uniformities cause a more noticeable problem. The two primary causes of non-uniformities are uniform detection efficiency and position dependent collection of the scintillation light, the former arising from each Photo-Multiplier (PM) tube having small differences in the pulse height spectrum. The latter arises from events that do not occur directly over the center of the PM tube, events may occur anywhere and will presumably often occur over the gaps and dead areas between the PM tubes.

The collimator is the weak link in the performance of a γ imaging system. For this reason, collimators are designed and chosen carefully depending on requirements. According to Cherry et al. collimator resolution R_{coll} is defined as the Full Width at Half Maximum (FWHM) of the radiation profile from a point or line source of radiation projected by the collimator onto the detector [3]. This profile (see Figure 3.1) is also called the Point or Line Spread Function (PSF & LSF) and in its simplest form is given by:

$$R_{coll} \approx d(l_{eff} + b)/l_{eff} \tag{3.2}$$

where

- b is distance from the radiation source to the collimator.
- d is the diameter.
- l is the real length (see Figure 3.1).
- $l_{eff} = l - 2\mu^{-1}$ is the effective length of the collimator holes.
- μ is the linear attenuation coefficient of the collimator material.

The problem of determining the original image distribution is aided by knowledge of the PSF. A PSF is analogous to a time impulse response for a physical system except that it provides spatial characteristics for an imaging system. The PSF provides information about the form of distortion that the original image distribution has undergone. This is critical knowledge in the image restoration process. A prior

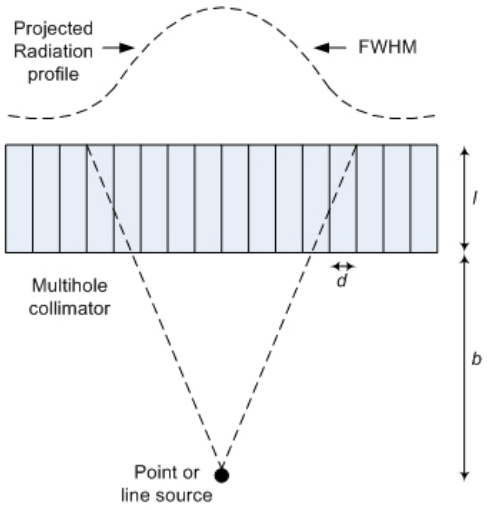

Figure 3.1: Adapted from *Physics in Nuclear Medicine* [3] this image depicts the Point Spread Function also known as the radiation profile.

knowledge of the PSF is required if it is to be applied in the deconvolution process associated with image restoration. There are, however, conditions for image restoration filters to be successful. These include the shift invariance of the PSF, radial symmetry and PSF uniformity with source depth [8]. The distortion is a function of the particular imaging system and will differ among imaging systems. The origins of this distortion can be attributed to transformations by the imaging system causing radiometric distortions (sensor non-linearities etc.) [9].

The PSF is represented as a matrix that when convolved with an ideal image f will produce the recorded image g (assuming no added noise). A major assumption often used when attempting to de-blur images is that the distortion is space-invariant or shift-invariant. In NM there is approximate radial symmetry but unfortunately there is shift variance as well as PSF non-uniformity with source depth. In this study, shift invariance is assumed, and because source depth is more or less known by NM physician the PSF matrix can be adjusted accordingly. This allows for visually optimum image restoration in *planes of interest*. The concept of *planes of interest* will be further discussed in Section 6.1.1.

3.3 Noise Determination

Most image restoration techniques require a value of noise variance (σ_o^2) in order to operate correctly. In NM an approximate value for σ_o^2 can be determined using a flood source scan by a γ-camera. Iterative image restoration techniques that gradually remove the noise implies the original value of the noise variance will become redundant after the first iteration. A more accurate value of the up-to-date noise variance σ_i^2 at each iteration often results in superior image restoration.

There are many different methods used to update the value of σ_i^2, such as $Median/3\sigma$ *clipping method*, *block method* and *iterative multiresolution support method* [10]. Noise is characterized by its standard deviation. There are numerous ways of estimating standard deviation for a Gaussian distribution. Olsen experimented with six different methods and determined that the most accurate is the average method [11]. The average method involves filtering the image with an average filter and then subtracting the original image from its average. Image edges do not contribute to the estimate as they are disregarded if above a certain threshold determined from a cumulative histogram of magnitude of the intensity gradient. It is then possible to calculate an accurate estimate of the noise.

3.4 Data Models

Consistency of the image with apparent data is dependent on the specific data model chosen. It describes the probability of observing the data of the object that is in a particular state. It is a stochastic description of how the data is corrupted due to the noise. In this case it is given by the imaging system and is determined by inherent knowledge of the data model form and noise distributions. The noise distribution is defined by the detector noise. Detector noise can have many different aspects each with its own noise distribution or distortion.

There is inherent randomness in the number of γ-photons passing through the collimators. These quantum fluctuations can be accurately modeled as a Poission distribution and becomes approximately Gaussian for large counts. Also there is not a one-to-one correspondence between the number of incident photons and the number of charge carriers that are released. Many γ-photons are deflected or lost and some are randomly added. Finally, there is thermal noise in the electronics, that is characteristically assumed to be spatially uncorrelated and has a zero-mean

Gaussian with uniform "white" power spectrum [12]. Essentially the random noise associated with image formation can be described either with a Poisson or with a Gaussian distribution. The lower the data counts the higher the statistical noise [13]. In reality the projection data follows a Poisson distribution [13].

$$P(g|f) = \prod_i \frac{(\lambda f_i)^{g_i} exp(-\lambda f_i)}{g_i!} \tag{3.3}$$

where $p(g|f)$ is the conditional probability of g being a corrupted form of the ideal image f [5], g_i is the number of counts at the detector and f_i is the source density estimate at pixel position i. However, for the purpose of this discussion, we will model the noise as a Gaussian distribution specifically being additive, independent and with a stationary zero-mean. The probability in terms of a Gaussian distribution [14] with a standard deviation, σ, is given by Equation 3.4.

$$P(g|f) = \prod_i \frac{1}{\sqrt{2\pi}\sigma} exp(-\frac{(g_i - f_i)^2}{2\sigma^2}) \tag{3.4}$$

3.5 Summary of Image Restoration

This chapter identifies that there are many different aspects causing image degradation, and discusses numerous image restoration techniques used to attempt reversal of that degradation. NM images have particular characteristic distortions, some of these distortions are corrected automatically by gamma cameras while other distortions require further intervention. The two primary distortions that need to be corrected are the blur described by a PSF and the statistical noise described by a distribution and its variance. A discrete PSF and an approximate noise variance can be determined and defined in various manners. All these choices will have a sizable impact on the success of the image restoration.

Chapter 4

Review of Mean Field Annealing

4.1 Background

A good alternative to Simulated Annealing in optimisation problems related to Markov Random Fields (MRF) is the Mean Field Theory (MFT). It provides comparable performance while converging more rapidly. This dissertation will not go into the complexities of MFT but a clear and comprehensive discussion of MFT can be found in a text on statistical mechanics by Chandler [15].

MFA is based on MFT and uses Markov Random Fields in the image restoration process. On the topic of MRFs: according to Perez [16] "each random variable directly depends on a few other neighboring variables. From a global point of view, all variables are mutually dependent, but only through the combination of successive local iterations." This statement captures Markov-type conditional independencies among random variables. An image can be considered a Markov Random Field if the intensities of pixels surrounding a center pixel are dependent on that center pixel and not directly dependent on any other pixel. Due to the Markov-type interaction between pixel intensities a suitable deterministic or stochastic iterative algorithm can be devised, in our case this algorithm is MFA. MFA is based on the common principle that at each step just a few variables (in MFA: a single one) are considered, all the others being "frozen" [16]. Markovian properties then imply that the computations required remain local, i.e. that they only involve the neighboring variables as is the case with MFA.

NM images are assumed to be piece-wise continuous images and thereby produce Markovian neighborhoods. Markovian neighborhoods allows the representation of

images as MRFs [17]. MFA is based on the image restoration methodology of anisotropic diffusion. Anisotropic diffusion is the process of smoothing all image regions which are not considered edges while ignoring regions which are considered edges. Acton describes the Anisotropic diffusion process as yielding "intraregion smoothing, not interregion smoothing, by impeding diffusion at the image edges" [18].

The MFA algorithm makes use of two techniques to achieve image restoration. Gradient descent is used as the minimisation technique while a deterministic approximation SA is used for optimisation [19].

4.2 Simulated Annealing

Simulated Annealing is a method that is used to increase the probability of conveniently stepping over local minima and converge to a global minimum even in the case of non-convexity [6]. However, it is well know that the major disadvantage of Simulated Annealing is the large computational effort associated with it. MFA makes use of Mean Field Theory and Gibbs distribution to derive a deterministic approximation to Simulated Annealing. This approximation helps resolve the problem of the computationaly intensive Simulated Annealing. The simulated annealing concept comes from the mechanical process of annealing. It can be derived from two seperate perspectives: statistical mechanics [20] and information theory [7, 21].

SA was developed in 1983 [22] to deal with highly nonlinear problems. SA is a generalization of a Monte Carlo method for examining the equations of n-body systems consisting of states and frozen states [23]. Consider an annealing process where a melt (liquids or metals), which is initially at a high temperature and in a disordered state, is gradually cooled. As cooling continues the system gains increasing order and approaches a "frozen" ground state. During this cooling process the system is in approximate thermodynamic equilibrium and can be considered, if the annealing process is performed correctly, to be in the lowest energy state. If cooling is insufficient or the initial temperature is too low the system can form imperfections or become trapped in meta-stable states (local minimum). Franco Busetti explains SA with the following analogy. "SA approaches the global maximisation problem similarly to using a bouncing ball that can bounce over mountains from valley to valley. It begins at a high [energy state] which enables the ball to make very high bounces, which enables it to bounce over any mountain to access any valley, given enough bounces. As the temperature declines the ball cannot bounce so high, and

it can also settle to become trapped in relatively small ranges of valleys. A *generating distribution* generates possible valley states to be explored. An *acceptance distribution* is also defined, which depends on the difference between the function value of the present generated valley to be explored and the last saved lowest valley. The acceptance distribution decides probabilistically whether to stay in a new lower valley or to bounce out of it. All the generating and acceptance distributions depend on the temperature." It has been proved that by correctly controlling the rate at which the temperature is cooled, SA can find the global optimum [24]. This would in theory require infinite time, and so algorithms such as *Fast annealing*, *Very Fast Simulated Reannealing (VFSR)* [25] or *Adaptive Simulated Annealing (ASA)* [26] and *Mean Field Annealing* are all exponentially faster and overcome the infinite computational problem.

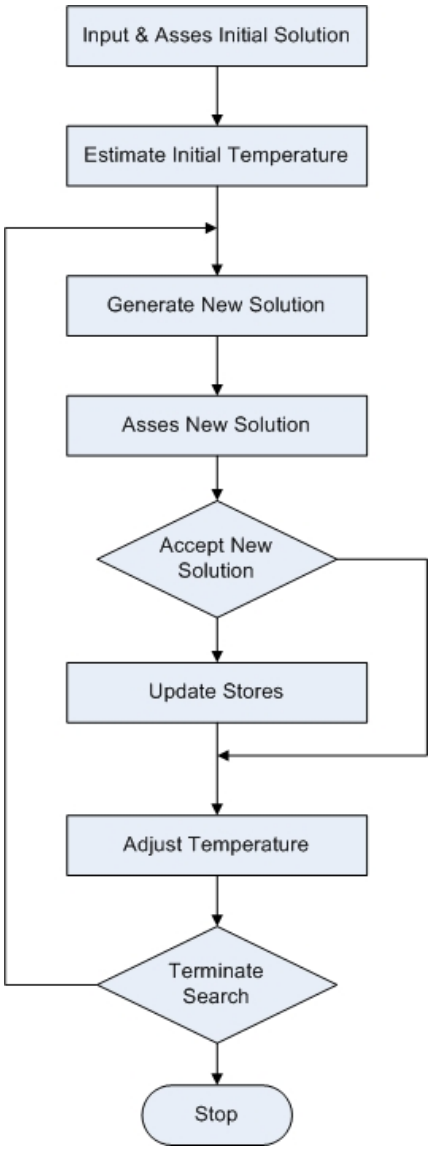

Figure 4.1: Generalised Simulated Annealing process flow chart [27].

As stated beforehand SA's one major advantage is that it does not become trapped in local minima, but it is also a robust and general technique. Besides the main computational disadvantage, SA is metaheuristic and delicate fine-tuning of parameters is required for successful operation [24]. The algorithm uses a random search that accepts changes that decrease an objective function f. It also accepts changes that increase it with a probability,

$$p = exp\left(\frac{-\delta f}{T}\right) \tag{4.1}$$

where δf is the increase in f and T is the control parameter, that is known as the system "temperature" and is irrespective of the objective function involved. This type of acceptance criteria is also seen in the Metropolis-Hastings algorithm which is a rejection sampling algorithm. Metropolis-Hastings is used to create a sequence of samples from a distribution $p(x)$ requiring only the density be calculated at x. This is used for probability distributions that are fundamentally difficult to sample. The algorithm makes use of Markov chains where each state is only dependent on its previous state. There are two types of Metropolis-Hastings algorithms, the "Random walk" and the "Independence chain". The latter can be more accurate but requires a priori knowledge [28]. It is this type of optimisation that Metropolis-Hastings algorithm is well suited for (see "Understanding the Metropolis-Hastings Algorithm" [29] for more information).

From a mechanical perspective: annealing subjects materials such as glass or metal to a process of heating and slow cooling in order to toughen and reduce brittleness. MFA has been shown to provide good results much faster than SA [30].

It has been employed in many different fields but particular to image processing, and has been used for; image restoration [30, 21, 31], motion estimation [32], image segmentation [33] and more [34, 35].

4.3 The Bayesian Approach

A Bayesian approach is used to develop the Objective Function defined in Section 4.6. Figure 4.2 illustrates a typical Bayesian mode approach.

θ - Random field model parameters

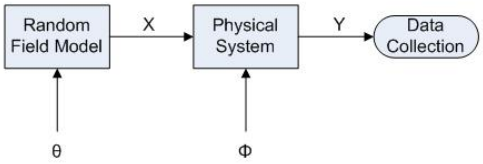

Figure 4.2: Bayesian model approach adapted from Bouman [36].

X - Unknown image

ϕ - Physical system model parameters

Y - Observed data

A random field may model the following:

- Achromatic/color/multispectral image
- Image of discrete pixel classifications
- Model of object cross-section

The Bayesian approach makes assumptions about the prior behavior. It does this by using a model that is problem dependent. While a good prior model may improve accuracy extensively, a model mismatch can impair accuracy. For this reason a Bayesian approach is taken firstly when a model mismatch is tolerable, and secondly when accuracy without the prior is poor [36].

According to Bayes' rule [37], the a-posteriori conditional probability $p(f|g)$ is given by:

$$P(f|g) = \frac{P(g|f)P(f)}{P(g)} \tag{4.2}$$

where:

$P(f|g)$ is the conditional probability that the measured image g is the corruption or distortion of the ideal image f.

$P(g|f)$ is the conditional probability or conditional density, that depends on the noise and blur processes.

$P(f)$ is the a-priori probability that is a measure of the form of f

$P(g)$ is the probability of producing the measured image g and is thus independent of f and is thereby treated as a constant. It is also known as the evidence.

The aim is to seek an estimate of f referred to as f^* that will maximise the posterior conditional probability [6]. This method is known as the Maximum A Posteriori method. That is Equation 4.2 must be maximised for image restoration. Although this can be achieved by numerous different methods, the Monte Carlo method may be suited to solving this type of computational problem because the problem is non-deterministic and stochastic in character. Monte Carlo methods are especially useful for modeling phenomena where there is a high degree of uncertainty in the systems inputs. Many degrees of freedom such as disordered materials, strongly coupled solids and liquids create computational problems that Monte Carlo methods excel at solving [38]. In this case the system would be the image with strong inter-pixel relationships coupled with external influences such as the noise and blur.

4.4 Noise Term

The conditional density is thus the probability of the noise and blur [6]. Assuming that the data model is sufficiently correct then the probability of $g_{i,j}$ given a pixel $f_{i,j}$ is influenced only by the distortion convolution factor h and the additive Gaussian white noise with zero mean and a variance σ^2. The conditional density for a (i, j) [6, 39, 40, 13, 41] is

$$P(g_{i,j}|f_{i,j}) = \frac{1}{\sqrt{2\pi}\sigma} exp\left[-\frac{\Big((f \otimes h)_{i,j} - g_{i,j}\Big)^2}{2\sigma^2}\right] \tag{4.3}$$

The noise and blur probability (conditional density) for the entire image [14, 41, 13, 5] can be written as

$$P(g|f) = \prod_{i,j} \frac{1}{\sqrt{2\pi}\sigma} exp\left[-\frac{\Big((f \otimes h)_{i,j} - g_{i,j}\Big)^2}{2\sigma^2}\right] \tag{4.4}$$

where i represents the horizontal coordinate and j represents the vertical coordinate.

4.5 Prior Term

In general images can be considered Markov Random Fields, meaning that each individual pixel intensity is dependent on its neighborhood of surrounding pixel intensities. A Markov Random Field may be characterized as a Gibbs distribution for the prior probability [42, 43]. The prior term represents our realizable knowledge of the attributes of the ideal image f [19, 41]. It is only dependent upon f and can be represented in the following form [32],

$$P(f) = \frac{1}{z} exp\left(\frac{-U(f)}{T}\right) \tag{4.5}$$

where z is the normalising function (also known as the partition function) and $U(f)$ is the energy function and is in the form of [6],

$$U(f) = \sum_{c} V_c(f) \tag{4.6}$$

When Equation 4.5 & 4.6 are combined they form the Gibbs (or Boltzman) distribution. Configurations of lower energies are more probable whereas configurations that correspond to higher energies are less likely [16]. In Equation 4.6 c stands for cliques and represents the set of neighborhood pixels and $V_c(f)$ is given by [6]

$$V_c = -exp\left[-\frac{\left(f_{i,j} - f_{i',j'}\right)^2}{2T^2}\right] \tag{4.7}$$

where $f_{i',j'}$ represents a pixel inside the clique set. Each clique is symmetric and therefore may be changed from an index set of cliques to pixels [6]. The prior term can then be expressed for a pixel $f_{i,j}$ inside f as [14, 19, 13]

$$P(f_{i,j}) = exp\left[-\frac{1}{T}\sum_{c} -exp\left(\frac{\left(f_{i,j} - f_{i',j'}\right)^2}{2T^2}\right)\right] \tag{4.8}$$

Equation 4.8 may be written in terms of a gradient operator $\Lambda_{i,j}$ instead of cliques. The summation sign falls away due to the gradient operator being a scalar measure of the brightness variation about pixel i, j. Simplifying and writing equation 4.8 for

an entire image f results in [14, 13, 39, 7]

$$P(f) = \prod_{i,j} exp\left[\frac{1}{T} exp\left(\frac{-\Lambda_{i,j}^2}{2T^2}\right)\right] \tag{4.9}$$

4.6 The Objective Function

Inserting Equation 4.4 & 4.9 into Equation 4.2 we have the following result [6],

$$P(g|f) \propto \prod_{i,j} \frac{1}{\sqrt{2\pi}\sigma} exp\left[-\frac{\Big((f \otimes h)_{i,j} - g_{i,j}\Big)^2}{2\sigma^2}\right] \times \prod_{i,j} exp\left[\frac{1}{T} exp\left(\frac{-\Lambda_{i,j}^2}{2T^2}\right)\right] \tag{4.10}$$

4.6.1 The Hamiltonian

The prior & noise term equations have been derived above; the successful restoration of images requires that Equation 4.10 be maximised. This ensures that the restored image has the maximum probability of being in the form of the scene f while still minimizing the amount of noise in an image by smoothing it. The ratio between these two concepts will be referred to as β. This problem of maximization can be turned into a problem of minimisation by taking the natural logarithm and changing the sign of Equation 4.10. The resulting term is the new objective function and will be referred to as the Hamiltonian. The Hamiltonian (H) can generally be interpreted as representing the energy of a physical system. H is then the sum of the kinetic and potential energy [44]. In this case we are not dealing with a physical system but rather an image whose pixels contain and interact "energetically". We now refer to the energy of an image by examining its prior and noise terms. These two terms will be examined further in this chapter.

The Hamiltonian is constructed from both the prior and noise term and is derived as follows [6, 7, 13, 5, 19],

$$H_T(f) = -ln[P(g|f) \times P(f)] \tag{4.11}$$

$$H_T(f) = -ln[P(g|f)] - ln[P(f)] \tag{4.12}$$

$$H_T(f) = \underbrace{-\sum_{i,j} ln\left(\frac{1}{\sqrt{2\pi}\sigma}\right)}_{Constant\ term} + \underbrace{\sum_{i,j} \frac{1}{2\sigma^2}\left((f \otimes h)_{i,j} - g_{i,j}\right)^2}_{H_n} + \underbrace{\sum_{i,j} -\frac{1}{T} exp\left(\frac{-\Lambda_{i,j}^2}{2T^2}\right)}_{H_p} \tag{4.13}$$

Writing Equation 4.13 in terms of the estimated image f^*, ignoring the constant term and adding in the ratio constant β, the following final objective function (referred to as the Total Hamiltonian) is derived,

$$H_T(f^*) = \underbrace{\sum_{i,j} \frac{1}{2\sigma^2}\left((f^* \otimes h)_{i,j} - g_{i,j}\right)^2}_{H_n} + \beta \underbrace{\sum_{i,j} -\frac{1}{T} exp\left(\frac{-\Lambda_{i,j}^2}{2T^2}\right)}_{H_p} \tag{4.14}$$

The Prior Hamiltonian H_p, also referred to as the penalty function, takes the form of an inverted Gaussian function. This is necessary to facilitate penalizing the image at its edges. This is a graduated process whereby the more pronounced the edge the greater the penalty. Penalizing means that there will be less smoothing over a region determined as an edge. This is as opposed to a region that is determined as a non-edge which will gain significant smoothing. Substantial literature [45, 46, 47, 48] has shown that the inverted Gaussian function (also known as the "upside-down Gaussian function") produces noise elimination without the blurring of considerable edges. The inverted Gaussian function is shown in Figure 4.3 and is conceptualized if viewed in the x-z plane.

The penalty function H_p is also a function of the 'temperature' T. The temperature is the variable that controls how much smoothing occurs at non-edges. T starts high and is gradually reduced. Consider Equation 4.14, when the temperature T is very high the prior term H_p can be essentially ignored [49]. The minimization process thus becomes Maximum Likelihood (ML) restoration. As seen from Figure 4.3 high temperatures result in almost no penalty for edges as well as non-edges. As the temperature is reduced, gradients 'close' to zero (homogeneous regions) are penalised to a greater extent. It is noteworthy that it is the inverted Gaussian function that defines which gradient magnitudes are considered 'close' to zero. Besag [45] explains

that the prior "should be strictly increasing" in the absolute value of $\Lambda_{i,j}$ and if "occasional abrupt changes" are expected, it should rapidly reach a maximum. This criterion is also covered by Geman & McClure [47] and Hebert & Leahy [48] and Blake & Zisserman [46] achieve a similar result by using a "clipped parabola". The reduction of T and the use of the inverted Gaussian function achieves three goals,

- The algorithm becomes progressively stricter as to what it considers an edge and a non-edge
- Non-edges are gradually assigned a greater negative number and thus experience a greater smoothing affect
- Allows the algorithm to skip local minima and to minimise to the global minimum

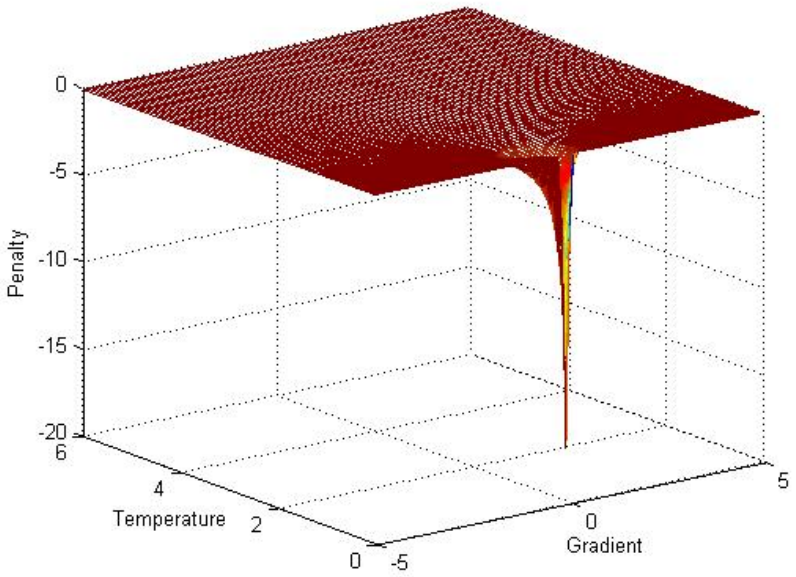

Figure 4.3: Three dimensional interpretation of how the penalty function changes the penalty depending on the temperature and gradient.

Snyder et al. puts it eloquently [6]: "It is comforting that the result of the MAP (Maximum A-posteriori Problem) formulation results in an objective function so intuitively correct: the "noise term", H_n, simply says that the restored image f^* should resemble the measured image g. The prior term H_p simply says the restored image should be smooth except for abrupt discontinuities at edges."

4.6.2 Gradient Operator

An edge point can be regarded as a point in an image where a discontinuity (in gradient) occurs across some line [50]. A discontinuity may be classified as one of the five types seen in Figure 4.4.

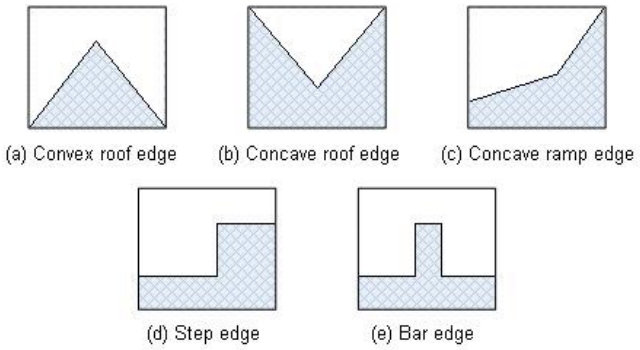

Figure 4.4: Different discontinuities associated with an edge (Adapted from Vision Systems [50]).

A gradient discontinuity can be defined where the gradient of the pixel values change across a line. This type of discontinuity can be classed as

- *roof* edges (display second order characteristics)
- *ramp* edges
- *convex* edges
- *concave* edges

There are many different types of first order edge operator convolution masks, such as *Roberts Cross* [51] and *Sobel* edge operator [52] convolution masks. First order operators all approximate *first order derivatives* of the pixel values in an image.

The *Sobel edge operator* is an important edge operator that is often used. Like the *Roberts Cross* operator *Sobel* uses two convolution masks given by

$$\mathbf{\Delta_x} = \begin{pmatrix} -1 & 0 & 1 \\ -2 & 0 & 2 \\ -1 & 0 & 1 \end{pmatrix} \quad \mathbf{\Delta_y} = \begin{pmatrix} 1 & 2 & 1 \\ 0 & 0 & 0 \\ -1 & -2 & -1 \end{pmatrix} \tag{4.15}$$

Sobel masks are 3×3 while Roberts Cross are 2×2. An advantage of using a larger mask size is that errors due to the effects of noise are reduced by local averaging within the neighborhood of the mask. Another advantage is the use of a mask that is odd sized because the operators are centered and can therefore provide an estimate that is biased towards a center pixel (i, j) [53].

It is also possible to use *second order derivatives* to detect edges. A very popular second order operator is the Laplacian operator. The Laplacian of a function $f(x, y)$, denoted by $\nabla^2 f(x, y)$ is defined by [54]:

$$\nabla^2 f(x, y) = \frac{\partial^2 f(x, y)}{\partial x^2} + \frac{\partial^2 f(x, y)}{\partial y^2} \tag{4.16}$$

Using discrete difference approximations to estimate the derivatives and represent the Laplacian operator with a 3×3 convolution mask is:

$$\nabla^2 \mathbf{f}(\mathbf{x}, \mathbf{y}) = \begin{pmatrix} 0 & 1 & 0 \\ 1 & -4 & 1 \\ 0 & 1 & 0 \end{pmatrix} \tag{4.17}$$

There are disadvantages to using second order derivatives.

- Second derivatives will exaggerate noise more than first order operators, and can be inconvenient when dealing with high noise high energy (such as Gallium) Nuclear Medicine images.
- No directional information about an edge is available with second order operators.

Interestingly, Brady et al. [53] says "that humans usually do not show strong directional preferences when detecting edges, motion, or reflective boundaries."

Due to these disadvantages, methods such as Laplacian Of Gaussian (LOG) have been developed that blurs the image. Blurring allows for zero-crossing at the edge while edge position is still preserved [53]. There are many other methods in use today such as the Difference Of Gaussian (DOG) operator (evidence exists that this is similar to the human visual system) and the more common Canny edge detector [55].

A more stable [53] method called the Quadratic Variation Operator is implemented in this study. The continuous Quadratic Variation Operator is given by [54]:

$$\Lambda_{i,j}^2 = \left(\frac{\partial^2 f}{\partial x^2}\right)^2 + \left(\frac{\partial^2 f}{\partial y^2}\right)^2 + \left(\frac{\partial^2 f}{\partial xy}\right)^2 \tag{4.18}$$

that according to Wang et al. [19] can be implemented by convolving the following three kernels as follows [14]

$$\Lambda_{i,j}^2 = (f \otimes q_{xx})^2 + (f \otimes q_{yy})^2 + (f \otimes q_{xy})^2 \tag{4.19}$$

where

$$\mathbf{q_{xx}} = \frac{1}{\sqrt{6}}\begin{bmatrix} 0 & 0 & 0 \\ 1 & -2 & 1 \\ 0 & 0 & 0 \end{bmatrix} \quad \mathbf{q_{yy}} = \frac{1}{\sqrt{6}}\begin{bmatrix} 0 & 1 & 0 \\ 0 & -2 & 0 \\ 0 & 1 & 0 \end{bmatrix} \quad \mathbf{q_{xy}} = \frac{1}{2}\begin{bmatrix} -1 & 0 & 1 \\ 0 & 0 & 0 \\ -1 & 0 & -1 \end{bmatrix} \tag{4.20}$$

Wang [56] suggests using a first order gradient operator for piecewise uniform images and second order quadratic variation operator for piecewise linear images. This is intuitive because piecewise uniform images exhibit step edges and piecewise linear images exhibit roof edges displaying second order characteristics.

4.7 Gradient Descent

With continuous state space, all gradient descent techniques or iterative system solving methods can be used [16] as minimizing routines. With both discrete and continuous state spaces, the simple *iterated conditional modes* may also be used.

Gradient descent is an optimisation algorithm that approaches a local minimum of a function by taking steps proportional to the negative of the gradient or approximate gradient of the function at the current point.

Consider the current estimate of the image to be $f^* = f^k$, then the process of

minimization is given by [14]

$$f_{i,j}^{k+1} = f_{i,j}^{k} - \alpha \frac{\partial H_T(f^k)}{\partial f_{i,j}^{k}} \tag{4.21}$$

where

k represents the current gradient descent iteration

$H_T = H_n + H_p$ Equation 4.14

α is the *step size*

Y - Observed data

Two weaknesses of gradient descent are

- If the curvature in different directions is very different then gradient descent can take many iterations to converge toward a local maximum/minimum [57].
- Finding the optimal α per step can be computationally intensive. Conversely, using a fixed α can have poor results [57]. A small step size will converge to a minimum (however computationally expensive) and too large a step size may result in divergence [5].

A more powerful algorithm is given by the Broyden-Fletcher-Goldfarb-Shannon (BFGS) method that consists of calculating at every step a matrix that is multiplied by the gradient vector to go into a "better" direction, combined with a more sophisticated linear search algorithm to find the "best" value of α [58].

In gradient descent used for MFA, the parameter α needs to be recalculated at every step. There have been various recommendations as to how to calculate α. Bilbo et al.[20] recommends

$$\alpha = \eta \times \sigma \times \frac{\sqrt{T}}{RMS(d)} \tag{4.22}$$

where

η is a dimensionless variable [59] that depends on the rate of annealing ρ[1] where $\eta = 1 - \rho$

σ is the standard deviation associated with the image noise.

$RMS(d)$ is the root mean square norm of $\frac{\partial H_T(f^k)}{\partial f^k_{i,j}}$

Another version of determining α is suggested by Wang [56],

$$\alpha = \sqrt{\frac{T}{T_{final}}} \times \frac{\bar{x}}{|\nabla H|} \times N \times \eta \times \kappa \times \gamma \tag{4.23}$$

where

N is the total number of pixels in the image

$|\nabla H|$ is the total change in the Hamiltonian (in the previous iteration)

$\bar{x}$ is the average pixel value

κ is the relaxation ratio that is empirically determined for each type of image

γ is a factor that is dependent on the change in the Hamiltonian and is used to control the step size where if $H(f^{k+1}) > H(f^k)$ then γ is set to 0.5 to ensure gradient descent. When $H(f^{k+1}) < H(f^k)$ then γ is maintained at 1.

4.7.1 Partial Derivative

As evident from Equation 4.21 the partial derivative of the Total Hamiltonian (Equation 4.14) is required to complete the gradient descent algorithm [14].

$$\frac{\partial H_T(f^k)}{\partial f_{i,j}} = \frac{\partial H_n(f^k)}{\partial f_{i,j}} + \beta \frac{\partial H_p}{\partial f_{i,j}} \tag{4.24}$$

The partial derivative of the Noise Hamiltonian is easily derived [5] for a single pixel (i, j) as

$$\frac{\partial H_n(f^k)}{\partial f_{i,j}} = \frac{1}{\sigma^2} \left(\left(f^k \otimes h \right)_{i,j} - g_{i,j} \right)^2 \otimes h_{rev} \tag{4.25}$$

[1] ρ is the ratio at which the temperature, T, is decreased each MFA iteration and will be discussed in greater detail in section 4.8 on page 26.

Combining H_p from Equation 4.14 and the edge operator for continuous quadratic variation Equation 4.18 the following expression for H_p[2] is derived

$$H_p = -\frac{1}{T} exp\left(-\frac{(f \otimes q_{xx})^2 + (f \otimes q_{yy})^2 + (f \otimes q_{xy})^2}{2T^2}\right)_{i,j} \tag{4.26}$$

Determining the partial derivative of the Prior Hamiltonian of the form of Equation 4.26 is thus given by [5]

$$\frac{\partial H_p}{\partial f_{i,j}} = \left(\frac{\partial H_p}{\partial f_{i,j}}\right)_{xx} + \left(\frac{\partial H_p}{\partial f_{i,j}}\right)_{yy} + \left(\frac{\partial H_p}{\partial f_{i,j}}\right)_{xy} \tag{4.27}$$

where [5]

$$\left(\frac{\partial H_p}{\partial f_{i,j}}\right)_{xx} = -\frac{1}{T^3}\left(\left((f \otimes q_{xx})\, exp\left(-\frac{(f \otimes q_{xx})^2 + (f \otimes q_{yy})^2 + (f \otimes q_{xy})^2}{2T^2}\right)\right) \otimes q_{xxrev}\right)_{i,j} \tag{4.28}$$

Similar expressions can be found for $\left(\frac{\partial H_p}{\partial f_{i,j}}\right)_{yy}$ and $\left(\frac{\partial H_p}{\partial f_{i,j}}\right)_{xy}$

Bilbro et al. [7] found a superior model is achieved using

$$\left(\frac{\partial H_p}{\partial f_{i,j}}\right)_{xx} = -\frac{1}{T^3}\left(\left((f \otimes q_{xx})\, exp\left(-\frac{(f \otimes q_{xx})^2}{2T^2}\right)\right) \otimes q_{xxrev}\right)_{i,j} \tag{4.29}$$

4.8 The MFA algorithm

The MFA algorithm is based on the equations and concepts derived in the previous sections. MFA for image reconstruction consists of the following primary steps shown in Figure 4.5. MFA consists of two primary calculation loops; the inner gradient descent loop and the outer annealing loop. The annealing process is primarily controlled by the temperature. The temperature is set at an initial value

[2] for a single pixel (i, j)

and an estimate of the image must be determined. The estimate of an image can be the recorded image or an already enhanced version (e.g. filtered) of the recorded image. The annealing loop performs two primary functions, viz. calling the gradient descent loop and gradually reducing the temperature [5]. The gradient descent loop re-evaluates the noise and prior Hamiltonian as well as their respective partial derivatives at this new reduced temperature. The gradient descent loop then performs gradient descent using the total Hamiltonian partial derivative and the parameter alpha. It then iterates until a stopping criterion has been met.

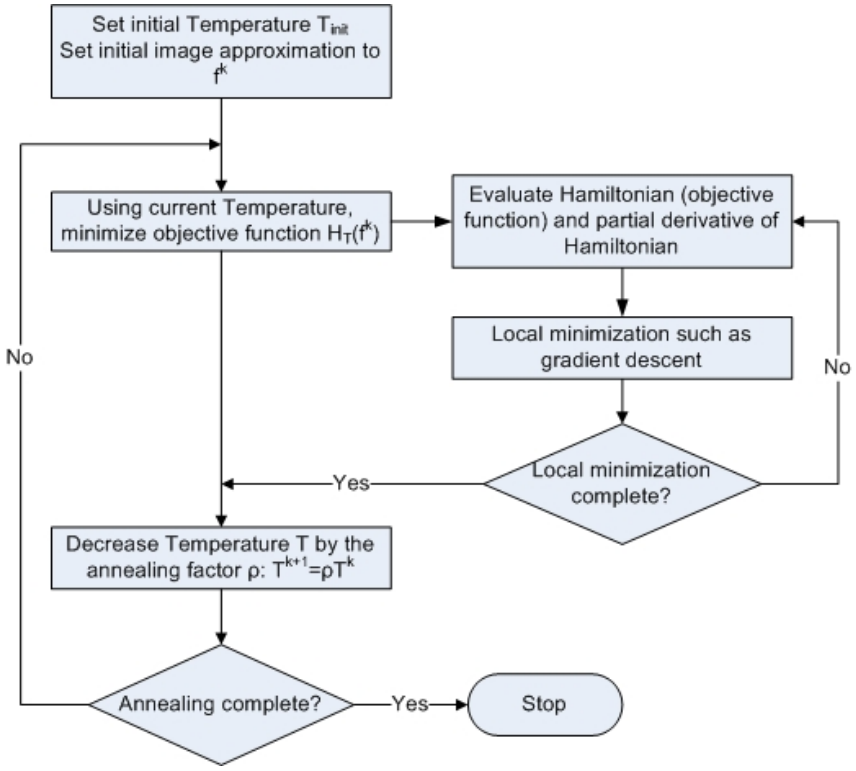

Figure 4.5: MFA process overview flow chart.

4.9 Summary of MFA

This chapter conducts a review of MFA, systematically stepping through the mathematical derivation of a MFA type algorithm. It describes in detail, but not in full, the requirements and choices that are needed for a successful outcome. MFA is a deterministic algorithm that uses anisotropic diffusion type methodology to improve images. MFA is based on SA, not requiring the large computational effort of SA, but still retaining the advantage of avoiding being trapped by local minima. The objective function is derived using a Bayesian approach. The objective function

is the Hamiltonian representing the "energy" of the image and constructed from a prior term (penalty function) and a noise term. The prior effectiveness is based to a large extent on the choice of gradient operator. The gradient operator is chosen according to the image's edge attributes and in this case the Quadratic Variation Operator is chosen to perform edge extraction. The noise term is also discussed and an equation using a Gaussian distribution as the conditional density is assumed.

Although, a choice of minimization techniques exists, Gradient Descent is applied as the iterative minimization routine used in this algorithm. Various derivations of the partial derivative and variables required in Gradient Descent are described, following suggestions made by MFA pioneers. Finally the chapter outlines the flow of the MFA algorithm that needs to be implemented computationally and efficiently for effective results.

Chapter 5

Digital Phantom Images

As proof of concept the MFA algorithm is first tested on simple digital phantom scenes. This also serves the secondary purpose of concluding the suitable parameters to be used in a MFA algorithm.

Firstly a digital phantom image needs to be generated. The development of image restoration algorithms is greatly aided by using standard digital phantoms with known properties. A well documented and used example is the Shepp-Logan phantom [60] containing ellipsis with different absorption properties that resembles the outline of a head. An image of the phantom is shown in Figure 5.1.

Figure 5.1: Modified Shepp-Logan digital phantom [61] often used in image enhancing studies.

The Shepp-Logan phantom was not used because it did not contain the low resolution detail that Nuclear Medicine clinical images exhibit. Instead more generalized digital phantoms containing many different elementary shapes, overlapping with various intensities were used.

Figure 5.2A and 5.2B are the two scenes created and used for algorithm construction. Figure 5.2A contains only vertical and horizontal step edges categorized by rectangles at different intensity levels. Figure 5.2B is similar but also includes ovals with

different intensity levels. Both images are not complete representations of NM real images as they do not contain roof or ramp edges that are typically found in NM. But due to the complexity in construction of a MFA algorithm, Figure 5.2A and 5.2B are a necessity used as a stepping stone.

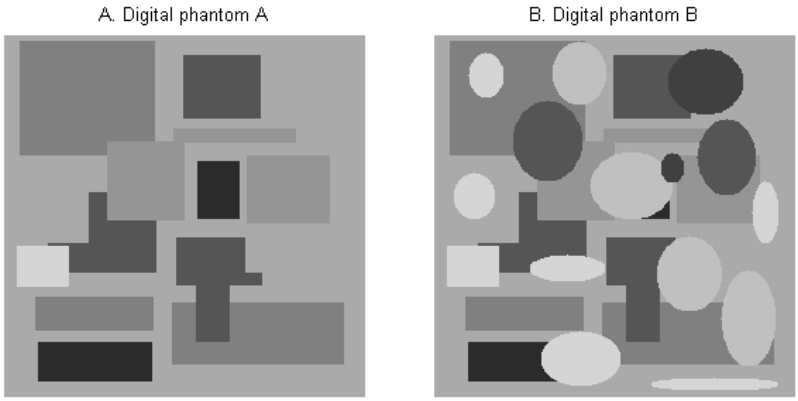

Figure 5.2: Two different digital phantoms used extensively in this project in the development of this MFA algorithm.

The next step is to degrade the image. According to Equation 3.1 the image must be distorted using a PSF and then noise must be added. The degraded digital phantoms can be seen in Section 5.4 Figure 5.3B.

5.1 Parameter Selection

One of the major downfalls with MFA is that there are many parameters (see list below) that are required for the algorithm to work successfully. Exacting logic to determine the optimal values of these parameters is difficult to derive, so an empirical approach is taken. Digital phantom images were used extensively in the development of a MFA algorithm and more pertinently in this discussion to determine the MFA parameters. Experimental empirical methods were used on numerous digital phantom images such as Figure 5.2A & B to determine optimal parameters. Also there are many different methods such as the various edge detection techniques that could all be used, but of these, some are more appropriate than others. The primary parameters and functions that need to be quantified for use in the MFA algorithm are the following [6, 17, 62, 7, 39, 5]:

- Edge Kernal Λ
- Beta β

- Starting Temperature T_{start}
- The annealing parameter ρ
- Stopping Temperature T_{stop}
- Calculation of Alpha α
- Gradient Descent Stopping condition

Since the best combination of the above parameters is not possible to determine mathematically, and is particular to each type of image, the following empirical approach is utilized: The MFA algorithm is looped many times and each time a different combination of parameters is used (see Appendix A). Once a set of results is attained the parameters providing the most significant improvement in the least number of iterations is chosen.

5.2 Determining Alpha

There is previous work done in determining the value of α required in Gradient Descent (see Section 4.7) for MFA application. However, in this study, Equation 4.22 used by Bilbro was found to take too many iterations to approach a global minimum when compared to Equation 4.23 suggested by Wang. Despite this, we found that Bilbro's suggestion seemed to always provide better overall results (ignoring the lengthy processing time). Experimentation in this study, focused specifically on 256×256 sized images, yielded a combination of the useful aspects of the previous two equations and resulted in the following successful solution for α,

$$\alpha = \eta \times \sqrt{\frac{\sigma^2 T}{norm\left(\frac{\partial H_T(f^k)}{\partial f^k_{i,j}}\right)}} \times \kappa \tag{5.1}$$

where κ typically is between 1 & 5 for optimum performance.

5.3 Stopping Criteria

A large part of achieving success with MFA is knowing when to stop the iterative loop process and post a result. It requires the correct stopping criteria specific to

each type of MFA problem. In the image restoration problem, having the original phantom and the degraded version of the phantom allows for comparison using error metrics such as Peak Signal to Noise Ratio (PSNR) and Root Mean Square Error (RMSE). These error metrics are used to evaluate the improvement of the image. This is not necessarily a true indication of image improvement because a PSNR may indicate a large reduction in noise but this reduction in noise may be accompanied by a loss in sharpness of the image. Regardless the RMSE or PSNR can be used as a guideline and is a very good indication in the reduction of noise.

In order to ascertain the correct parameters described in Section 5.1, the PSNR is taken as the measure of image improvement. This is done by comparing it to the original scene (bearing in mind that in real-life NM imaging, the scene is always unknown).

5.4 Results

Figure 5.3B shows a digital phantom that has been degraded using a noise variance of 0.035 and a Gaussian blur standard deviation, (σ) of 2. These values are typical of the degradation parameters in certain planar NM cameras found during experimentation in this study. It is evident from Figure 5.3A and D that the MFA algorithm with the correct parameters can reduce noise substantially without damaging edge integrity. Figure 5.3C shows a Wiener filter restored image. Comparative noise reduction and edge classification is evident from Figure 5.3E and F, that displays the Sobel edges of the Wiener and MFA restored images. Looking carefully at Figure 5.3B, C and D, it is noticeable that edges appear sharper in the original and Wiener images in certain regions compared to the MFA restored image. This implies that MFA has blurred the image slightly in regions. However since MFA has extensively reduced the noise without edge compromise, it is now possible to apply filters to further enhance image edges without amplifying the noise. A standard sharpening filter available in Matlab, w (Equation 5.2), is recommended to highlight the edges of clinical images. Many other standard image enhancing techniques may also be used for post-processing and future work in this field is suggested.

$$\mathbf{w} = \begin{pmatrix} -0.167 & -0.67 & -0.167 \\ -0.67 & 4.33 & -0.67 \\ -0.167 & -0.67 & -0.167 \end{pmatrix} \tag{5.2}$$

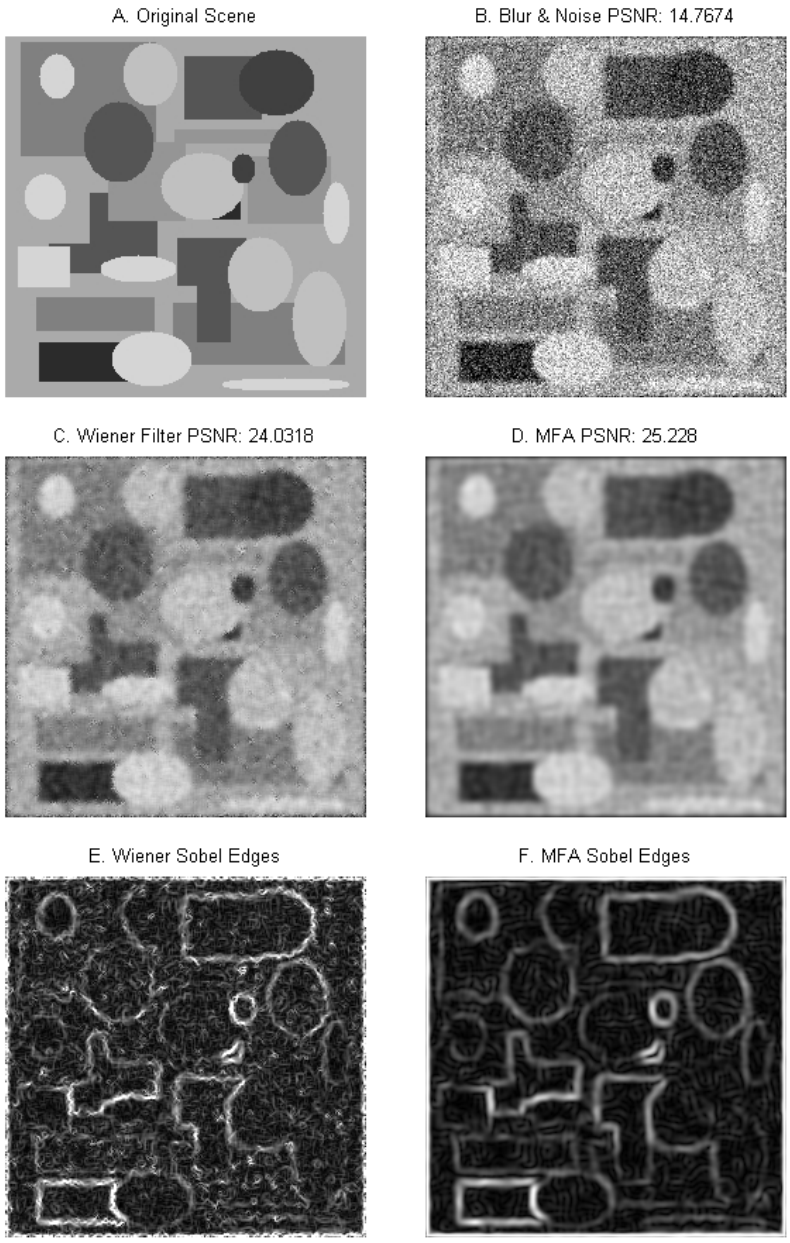

Figure 5.3: Comparison images of a digital phantom with an added noise variance of 0.035, a Gaussian blur standard deviation of 2 (hsigma) and PSF matrix size (hsize) of 5x5.

The image enhancement ability of MFA and comparison with the Wiener filter is also evident in Figures 5.4 & 5.5. These Figures show a cross section of the digital phantom in Figure 5.3 plotted against pixel intensity. They highlight the strengths of MFA, that can be categorized as a supplementary pre-filter image enhancing technique.

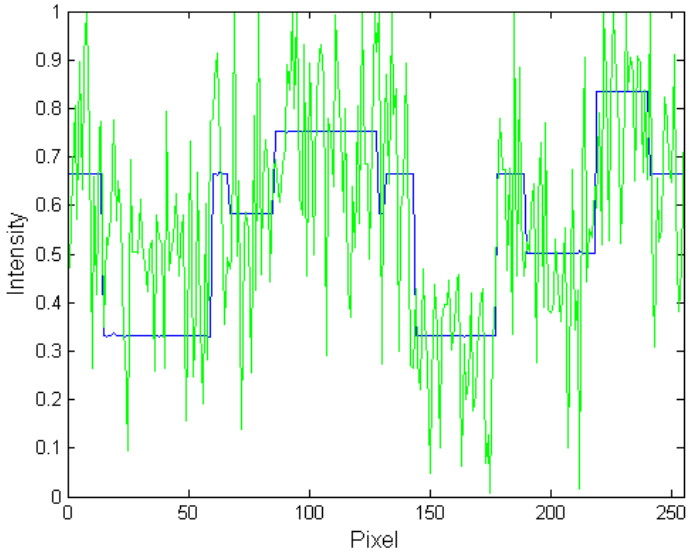

Figure 5.4: Graph showing a comparison between the original digital phantom (black curve) and the degraded version with a noise variance of 0.035, hsigma of 2 and hsize of 5x5 (green curve).

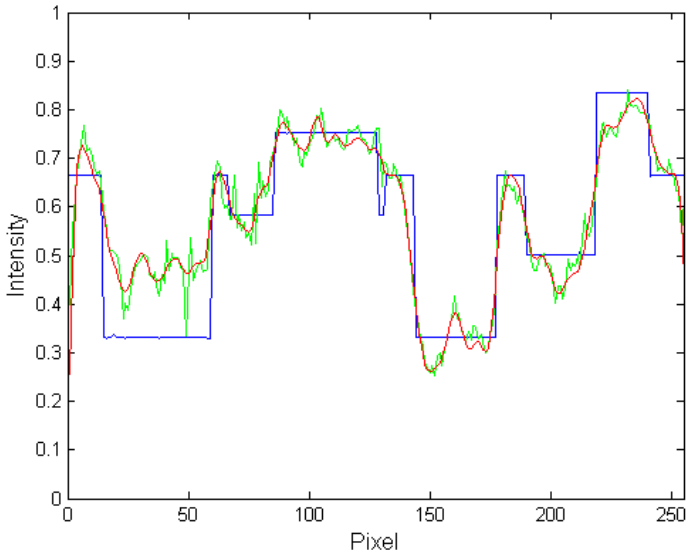

Figure 5.5: Graph showing a comparison between the original digital phantom and the Wiener restored version (green) and a MFA restored version (red).

5.5 Summary of Digital Phantom Images

Digital Phantom images are used as proof of concept when constructing an MFA type algorithm. They also help ascertain the correct parameters required for MFA.

The choice of parameter values and functions is critical in achieving successful results. This chapter highlights these parameters and summarises the techniques used to derive them. In particular the importance of the stopping criteria used when restoring digital phantom images is discussed as well as the issues when using these criteria for real images. Finally, the effective results are shown when applying this MFA algorithm to digital phantom images.

Chapter 6

Testing MFA on Clinical Images

6.1 Restoration Knowledge

The task of image restoration is to undo the effects of image blurring and additive noise. For this to be successful, information is required, namely the PSF and noise. The PSF can be estimated by imaging a small source of high intensity (in the case of NM imagery: a radiation source). The PSF can then be mathematically calculated from the results of the "point" source image. In NM, it is difficult to create a point source of radiation, therefore a line of radiation can be used instead. The PSF can still be derived and the mathematical determination is similar to that for a point source.

Although the PSF can be measured with reasonable accuracy (dependent on source depth), it is not possible to exactly determine the noise influence in a recorded image. However it is possible to establish the variance of the noise. The variance is determined by imaging a flood source of radiation. The recorded image can then be considered largely homogeneous and all variations in pixel intensity are assumed to make up the variance of the additive noise. Without knowing the scene of the image, a-priori of information about the degraded image has been gathered. It is this information that will be critical in the restoration process of the image to be described.

6.1.1 Determining the PSF

In NM images, as in many other images, the PSF frequently takes on the form of a Gaussian distribution. The PSF may be determined by examining a point source

image and fitting a Gaussian distribution to it. Since the PSF is continuous and the PSF representative matrix is discrete, appropriate approximations must be made when determining the size and values of the matrix. Once these approximations are made the PSF matrix is populated with an approximate Gaussian distribution.

Point and line sources need to be imaged in order to obtain the PSF. Firstly the point and line sources need to be created. The point sources were created by placing a small amount of Tc-99m into a small plastic tube (approximating a single point of intensity). The line source were created by using a test tube (1mm internal diameter) seen in Figure 6.1 filled with Tc-99m.

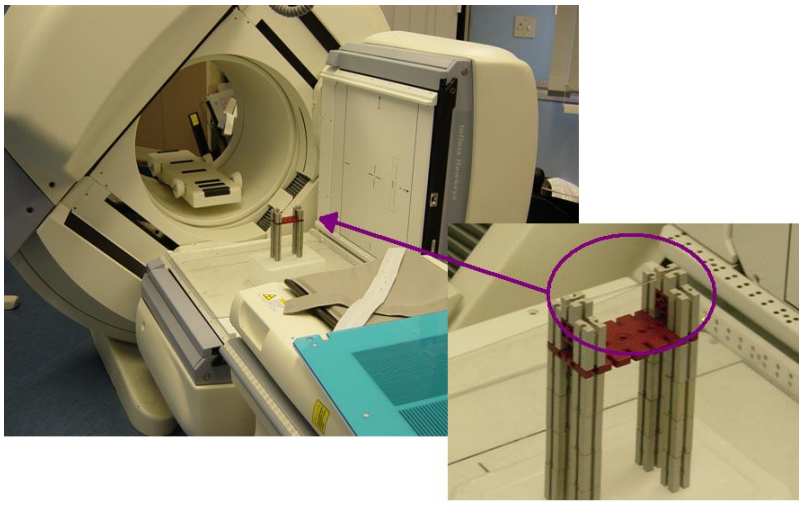

Figure 6.1: Photographs of how line sources were imaged in this experiment. The 1mm test tube contains Tc-99m and is imaged both vertically and horizontally at different distances parallel to the collimator surface.

To determine the PSF, point and line sources were placed at various distances away from the collimator. The PSF representative matrix values may also be confirmed by the LSF. Figure 6.2 shows the results of point sources and X & Y line sources imaged at 10, 15, 20 and 25cm from the collimator surface. By detailed inspection of the sources at the individual heights, approximate radial symmetry is concluded. This conclusion is not immediately evident, nor completely true. It is true that radiation events located directly over the center of the PM tube will exhibit radial symmetry. This being said, there are events that occur off-center (discussed in Section 3.2) resulting in between-pixel distributions, i.e. non-uniformity. If a point source is placed off-center from the PM tube, the resulting PSF image will exhibit a deformed Gaussian distribution. The deformation can be relatively greater for

radiation events occurring close to the collimator. This is problematic when attempting to ascertain the correct standard deviation of the Gaussian PSF. Every effort must be made to center a point source when determining a PSF. Although an image consisting of essentially countless off-center point sources will produce deformed Gaussian distributions, this does not adversely affect the image restoration process. This statement is justified in that an acquired image consists of many deformed Gaussian distributions added together producing primarily non-deformed Gaussian PSFs. The overall blurring affect is thus influenced by a correctly specified non-deformed PSF.

A simple check is performed by rotating the Y line source by 90 degrees and comparing it to the X line source. A discrete Gaussian distribution is fitted to the acquired point source. Vertical and horizontal line sources were imaged using capillary tubes to verify the point sources' distributions and to verify the approximate radial symmetry of the blur. Figure 6.3 shows how the point source is convolved with a line and then compared to the acquired line source. Ignoring the ends in the image of the capillary source, the two lines suffered only small differences with an RMSE of 5.5%, and that may be attributed to the noise. The process is repeated with the vertical line resulting in a RMSE of 4.8% that implies approximate radial symmetry. Radial symmetry and the fitted Gaussian PSF were verified at numerous distances. A visual example at 10cm and 20cm is provided in Figure 6.5 depicting how accurate the fitted PSF is compared to the acquired PSF.

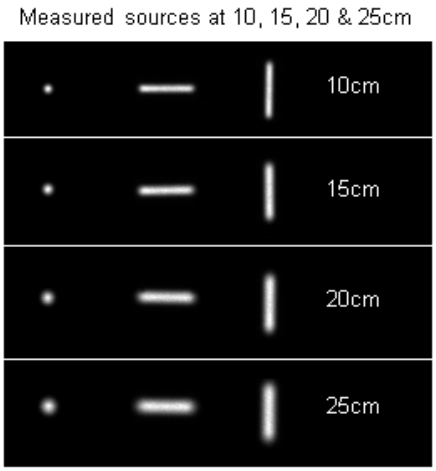

Figure 6.2: Imaged vertical and horizontal line sources with the respective point sources at 10, 15, 20, 25cm. These sources were acquired on a General Electric Healthcare Infinia gamma camera using a (Low Energy High Resolution) LEHR collimator.

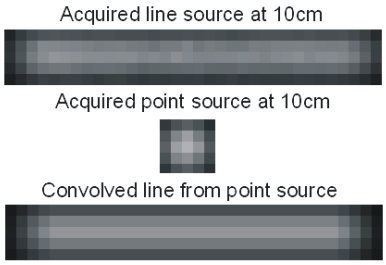

Figure 6.3: Visual comparison between a line source derived by convolving the imaged point source with a perfect line versus the imaged line source.

Figure 6.4 shows the Standard Deviation of the resulting fitted PSFs, and that these PSFs display a regional linear trend. A linear trend that has been fitted can be used to predict approximate PSFs at different distances from the collimator. This measured approximate linearity is consistent with Equation 3.2. From Figure 6.2 it can also been seen that the blur increases with source distance i.e. there is depth variance.

As mentioned, image restoration requires PSF uniformity with source depth [8]. Figure 6.2 clearly indicates that this is not the case and this disadvantage implies that the PSF will only be correctly specified for a single plane in the image. The other planes will experience a blurring effect due to the MFA process and an incorrectly specified PSF. This suggests that one could therefore select *planes of interest* by modifying the Gaussian distribution to define the PSF used in MFA. The *planes of interest* will experience image enhancement while the other planes may experience increased blur. Software running this image reconstruction technique would have to be flexible in terms of *planes of interest* and have easily adjustable PSF parameters.

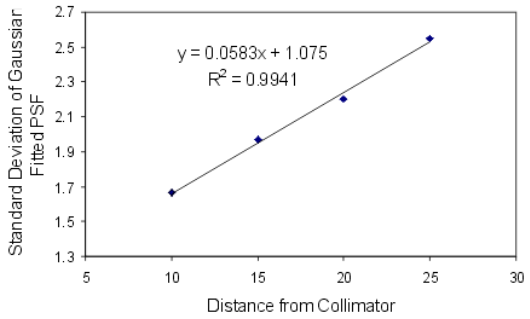

Figure 6.4: Derived values for standard deviation of the fitted Gaussian PSF using manual iterative techniques for a best fit solution.

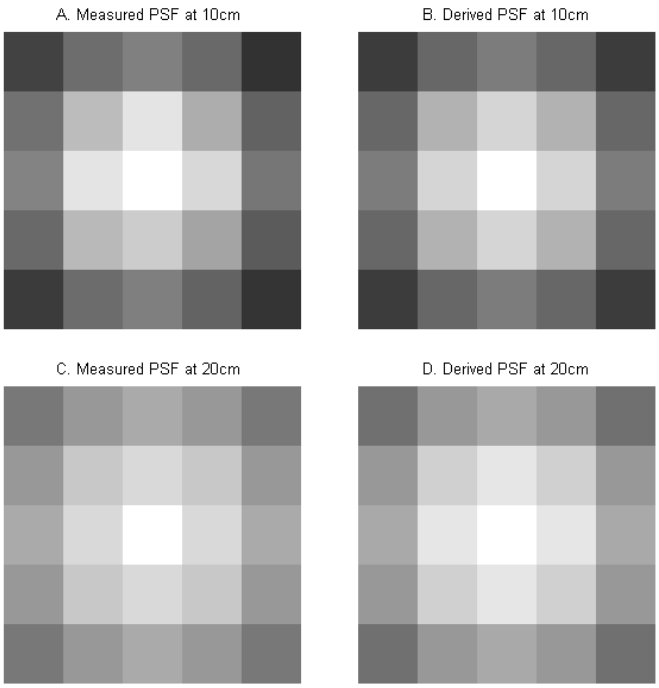

Figure 6.5: Visual comparison of the real and fitted point sources at 10cm and 20cm. The point sources have been zoomed for easier comparison.

6.1.2 Determining the Noise Variance

There are various methods of determining the noise variance of a NM image required in MFA. This determination can be accomplished by either using a flood source, pure computational methods or hybrid methods. Some examples of computational methods are listed in Section 3.3. Using a flood source and a novel computational method to obtain the noise variance is discussed below.

Flood Source

The process of MFA requires a value for the original noise variance (σ_o^2) in order to work successfully. An approximate value for σ_o^2 can be determined using a flood source scan by the camera (see Figure 6.6). Considering the process of MFA that gradually smooths the noise and sharpens the edges, the original value of the noise variance will become redundant after the first iteration of the MFA algorithm. A more accurate value of the up-to-date noise variance σ_i^2 results in the correct operation of the MFA algorithm.

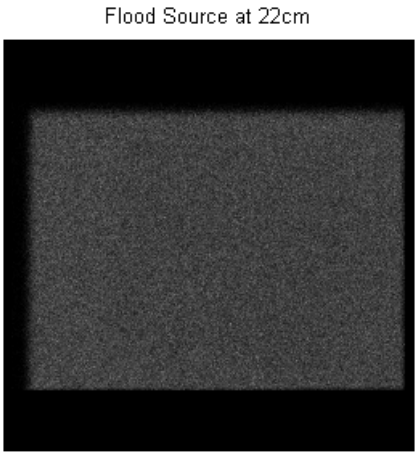

Figure 6.6: A flood source placed 22 cm from the collimator (LEHR) surface.

Quadtree Noise Variance Determination

A simple way of determining the σ_i^2 is by finding a homogeneous region of the image and estimating the noise only from this region. This method requires an initial guess that could be the noise value derived from a flood source or the previous noise value calculated. The methods discussed above are generalised and automatically determine the noise variance. This section discusses an alternative method of determining the noise variance of an image based on homogeneous regions.

Given that variance is defined as

$$\sigma^2 = \frac{1}{n-1}\sum_{i=1}^{n}(x_i - \bar{x})^2 \tag{6.1}$$

where the mean is given by

$$\bar{x} = \frac{1}{n}\sum_{i=1}^{n} x_i \tag{6.2}$$

Now consider that an image is made up of m number of homogeneous regions. A variance $\sigma_{\aleph}^2$ and mean $\bar{x}_{\aleph}$ can be calculated for each homogeneous region $\aleph$ where $\aleph = 1 \rightarrow m$. Once m number of variances have been calculated then the average or weighted average of these variances is computed. This is then an estimate of the noise variance of the image.

The definition of a homogeneous region is more complicated. A region must be considered homogeneous if the variance in pixel intensity is only due to noise and not due to image variation. All image information that varies by less than the noise variation is not distinguishable from the noise itself and therefore unrecoverable. If the pixel intensity does not vary by more then $3\sigma_{noise}$ within a specified region, then that region can be considered homogeneous [10, 63]. This presents a problem because σ_{noise} is unknown and is in fact what this algorithm is trying to determine. An optimisation method is then applied to overcome this problem.

1. Guess an average variance σ^2_{guess}.
2. Divide the image up into squares using quadtree decomposition with $3\sigma_{guess}$ as the threshold.
3. Calculate an average variance σ^2_{calc} of the m square homogeneous regions.
4. If $\sigma^2_{guess} \approx \sigma^2_{calc}$ then an estimate the noise variance has been computed. Otherwise take the next σ^2_{guess} as a value between the previous σ^2_{guess} and σ^2_{calc} and return to step 1.

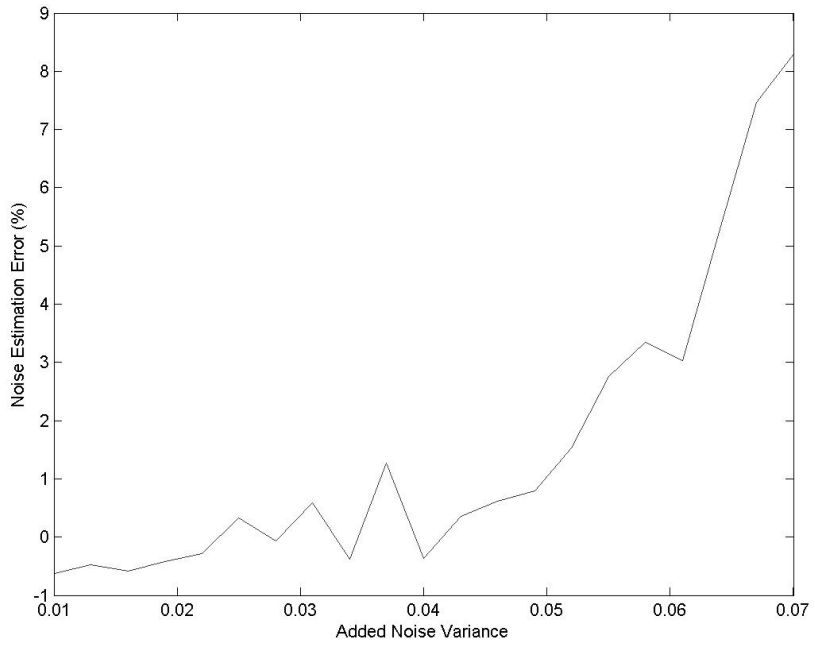

Figure 6.7: This graph depicts the resulting error in variance prediction using Quadtree noise determination techniques.

This algorithm is calculation-intensive, and performing it every MFA iteration creates a more computationally expensive algorithm (see Appendix A for details of the code). However the concept of recalculating the noise contribution at each MFA iteration is novel and further experimentation should be performed.

6.2 Discussion

The following technique was tested on a range of planar NM studies obtained from a GE Infinia γ-camera at Johannesburg Hospital. The use of clinical images in this study was approved by the Human Research Ethics Committee of the University of the Witwatersrand Johannesburg (protocol no. M060312). All images were anonymised.

A vital aspect of MFA is defining when the annealing process is complete. Excessive annealing will add significant blur to the image. Normally when dealing with digital phantom images, error metrics such as PSNR or RMSE may be used since the algorithm constantly compares the restored image with the real image. However, when dealing with NM images, this comparison cannot be made. The easiest solution would be to provide NM physicians with a movie of the restoration process and allow the NM physician to view and select the iterated image of choice (see Appendix B for further detail). NM physicians in general need to be careful in trading sensitivity of detection against false positive diagnosis. It is as yet unknown how using MFA in NM will affect the Receiver Operator Characteristic (ROC) curve that plots true positives against false negatives.

A more mathematical approach to achieving the correct stopping criteria is suggested by using the noise and prior Hamiltonians as enhancement indicators. During the testing and experimental phase, it was discovered that optimal visual annealing (in the experimental set) occurred between 23 and 28 iterations.

It is important to note that optimal annealing was judged by eye. MFA iterations 5, 15, 25, 35 and 50 are shown in Figure 6.8B,C,D,E and F respectively. Figure 6.8B shows the introduction of vertical and horizontal *fabric-like* artifacts. These artifacts can be attributed to the edge operator weaknesses, where at lower resolutions the Quadratic Variance Operator is more efficient at detecting vertical and horizontal edges as opposed to any edges that are obtuse. MFA skips this local minimum. Figure 6.8C illustrates how MFA has begun improving the image at 15 MFA iterations. Figure 6.8D shows what appears to be close to optimal visual improvement at 25

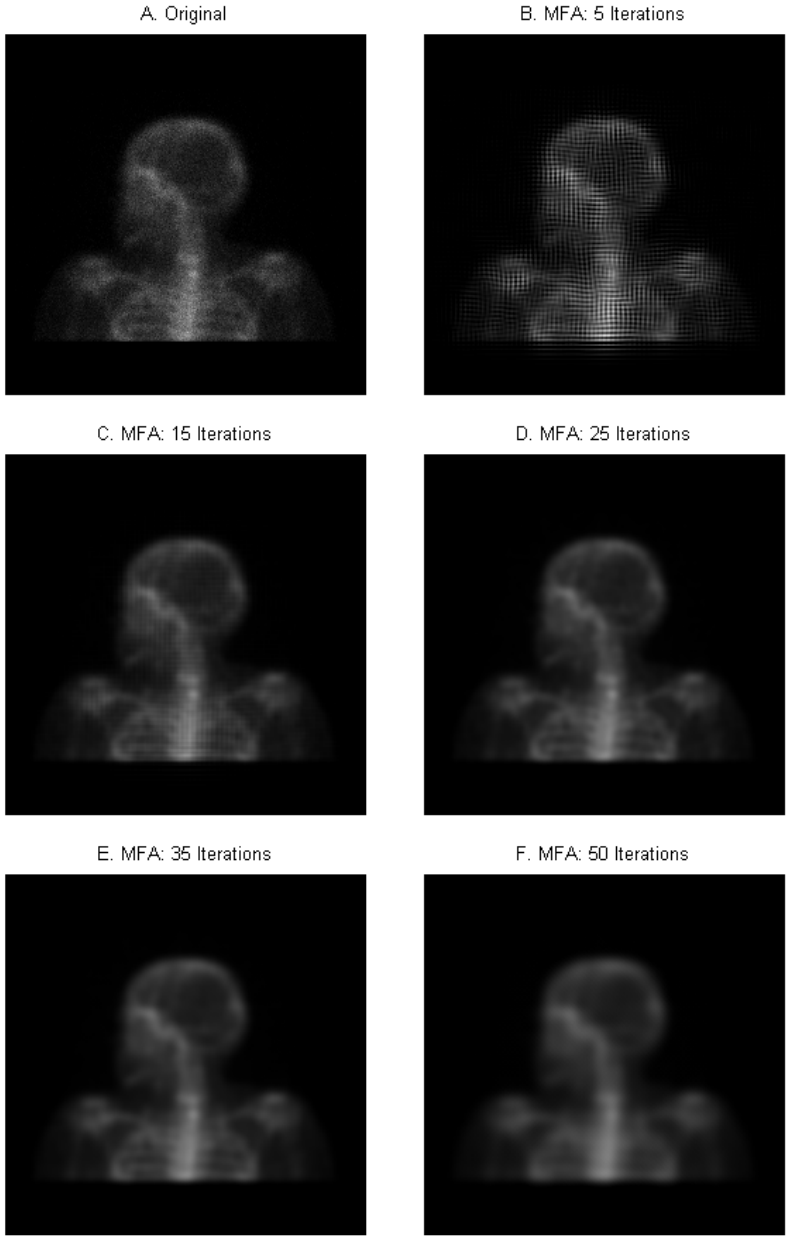

Figure 6.8: Shows iteration steps at 5, 15, 25, 35 and 50 for LLATS003 NM bone scan. Image D visually appears to be optimum.

MFA iterations and is otherwise currently unverifiable. The image appears to have blurred at this optimal point, however it is important to notice that this blur has occurred without edge compromise. Careful inspection shows that intra-region and NOT inter-region blurring has materialised from MFA restoration. The image can now be sharpened and restored using image enhancing techniques that are effective but highly sensitive to noise. Figures 6.8E & F clearly shows how the image begins to lose form due to over-annealing.

It was determined experimentally that MFA parameters for NM images are similar to those used in Figure 5.3D although they are not necessarily the optimal parameters. The following are the primary parameter specifications determined for visually optimal restoration (see Sections 4.7 and 4.8 for more detail):

- Beta coefficient of 100
- A starting temperature of $\sqrt{\sigma^2_{approx}} * 10$
- Gradient descent iterations 20
- Relaxation ratio of 2.5

Bar phantoms were initially used to try to quantify MFA improvement of clinical images. The idea is to put a radiation bath (flood source see Figure 6.6) behind the bar phantom and scan it to produce an image such as Figure 6.9. The method is to measure the FWHM resolution of the lines before and after MFA to characterize improvement. Only preliminary work has been undertaken and further work must be performed on this concept.

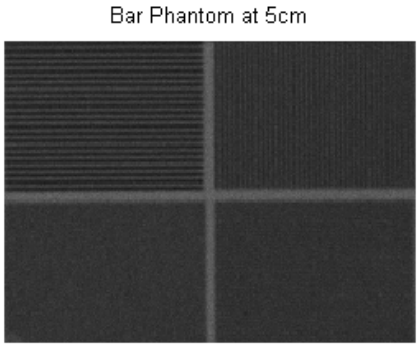

Figure 6.9: Bar phantom placed 5cm from collimator surface. Only the 4.23mm bars (top left) and 3.18mm (top right) appear. The 2.54mm (bottom right) and 2.12mm (bottom left) bars are not visually realisable.

The difference between optimal and sub-optimal appears to be negligible in this application of MFA. In this study the distance of the subject from the collimator is unknown, so a PSF with a standard deviation of 2 is chosen (corresponding to 17cm from the collimator see Figure 6.4). The noise variance is determined using a flood source as shown in Figure 6.6 and does not change with changing collimator distance. A variance of 0.035 is determined using the fact that a flood source is

considered a homogeneous region. Note that noise variance does change with image intensity scaling (during the image enhancement process) and this change must be factored in when applying MFA.

6.3 Results

Figure 6.10A shows an image acquired on General Electric Healthcare Infinia gamma camera. Figure 6.10C shows the restored image after 20 MFA iterations. The image appears to be slightly blurred with substantial reduction in noise. Figure 6.10E shows a Wiener restored image that looks very similar visually to the MFA restored image. The images are all optimally sharpened (by eye) using Equation 5.2 as the sharpening filter. The sharpening filter amplifies the noise in the original image after filtering the image only once as can be seen in Figure 6.10B. The sharpening filter is run three times on the MFA restored image with image enhancement occurring before noise amplification becomes apparent (Figure 6.10D). The result is a clearer and sharper image that may improve diagnosis. In contrast the sharpening filter can only be run twice before noise amplification becomes visually obstructive in the Wiener restored image seen in Figure 6.10F. Figure 6.10D appears to contain more viewable detail then Figure 6.10F.

As mentioned in Section 6.2 MFA results tend to exhibit *fabric-like* vertical and horizontal artifacts. After applying the particular sharpening filter (Equation 5.2), the artifacts become *fabric-like* diagonal. Further results are shown in Figures 6.11, 6.12, 6.13 and 6.14, all MFA enhanced images being iterated 25 times. These results also illustrate that these diagonal artifacts can be eradicated with minimal detail loss by using a [3x3] median filter.

It is possible that enhancing images using MFA may in fact introduce artifacts that may mislead diagnosis. Addition of detail that was not previously visible may require NM physicians to recalibrate how they assess their diagnosis. In the example (Figure 6.10), small focci of activity are seen in the skull after MFA and sharpening, that were not previously noticeable. It is uncertain if these represent real lesions or artifacts caused by the MFA approach, and further research would be required to come to a conclusion. MFA may also be much more effective and suitable for certain types of NM images. Figures 6.10, 6.11 and 6.12 show an increase in detail but this may not be the case for Figures 6.13 and 6.14. Further studies of large numbers of different types of NM images would be required to determine the usefulness of this image restoration technique. (see Appendix C for enlarged bone scan results)

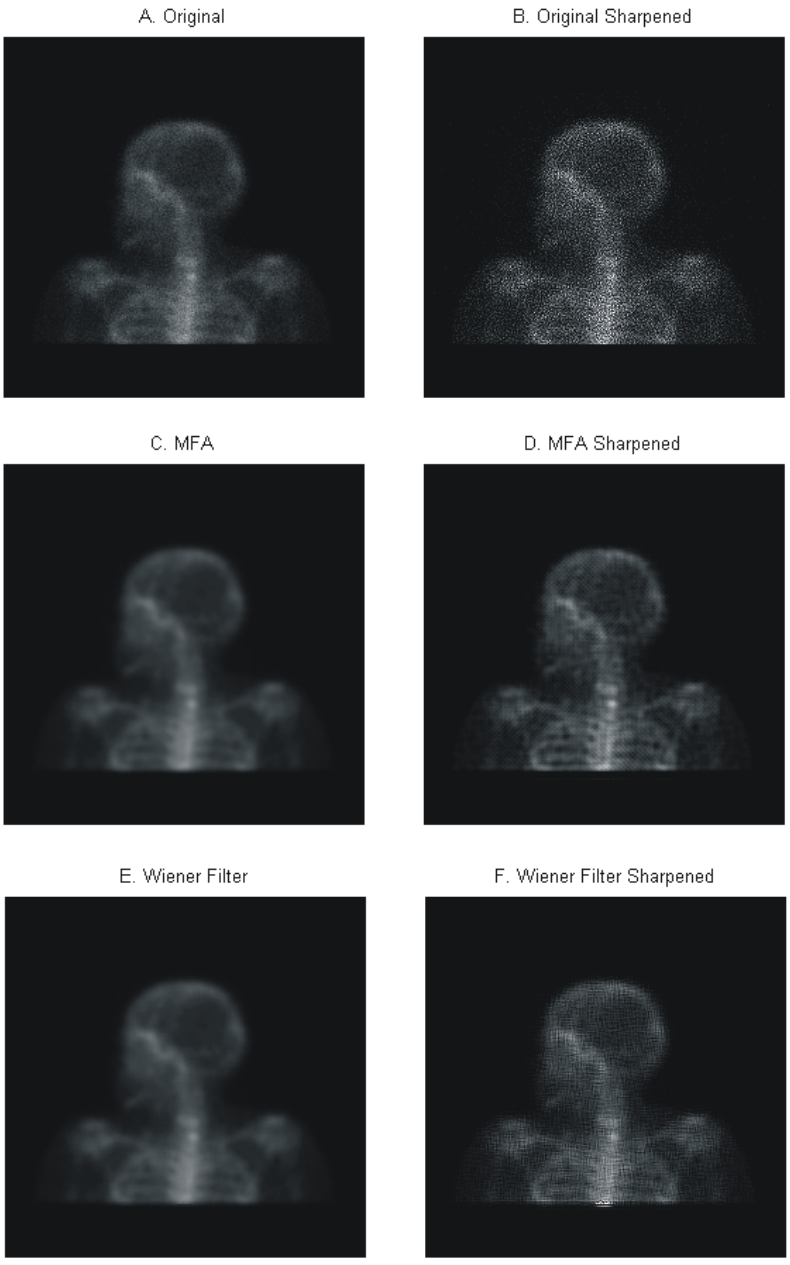

Figure 6.10: Results for LLATS. A:original bone scan, B: original scene sharpened, C: MFA result after 25 iterations, D: MFA result sharpened, E: Wiener filter result, F: Wiener filter result sharpened.

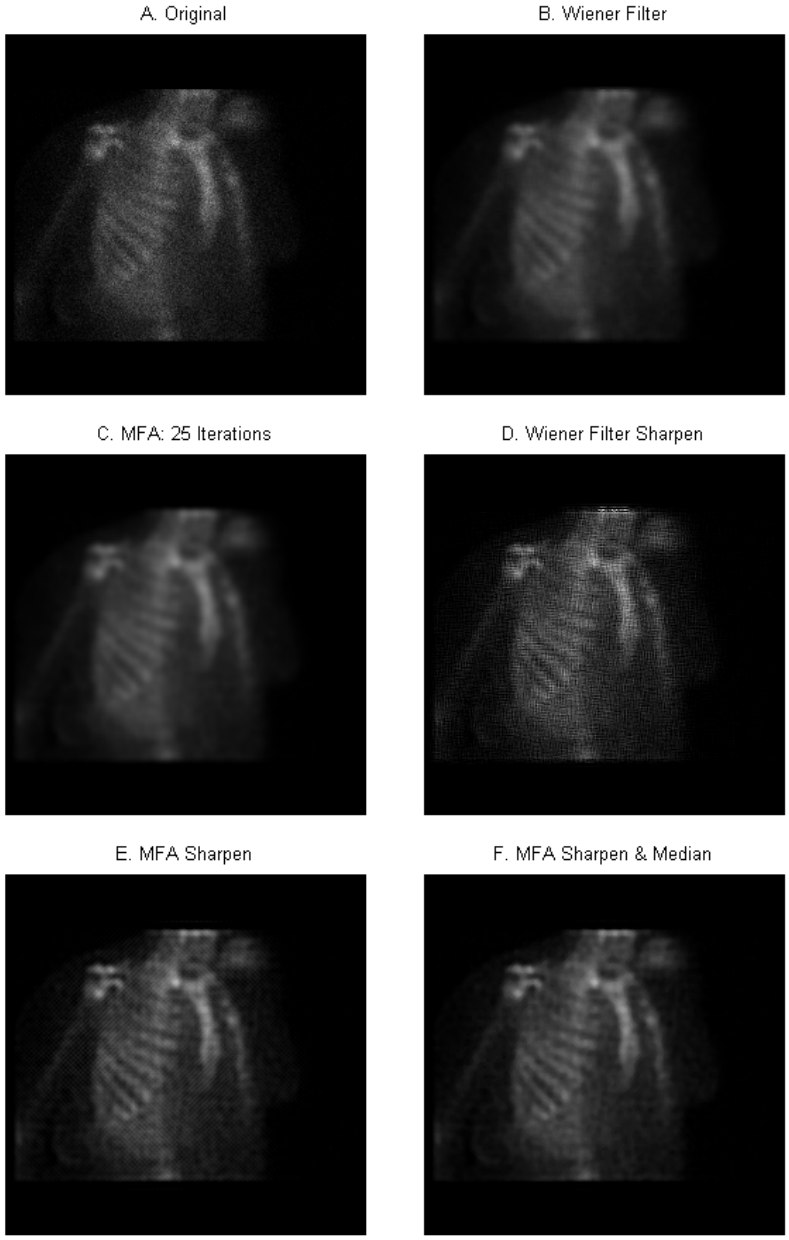

Figure 6.11: Results for LAO001. A:original bone scan, B: Wiener filter result, C: MFA result after 25 iterations, D: Wiener filter result sharpened, E: MFA result sharpened, F: MFA result sharpened and median filtered.

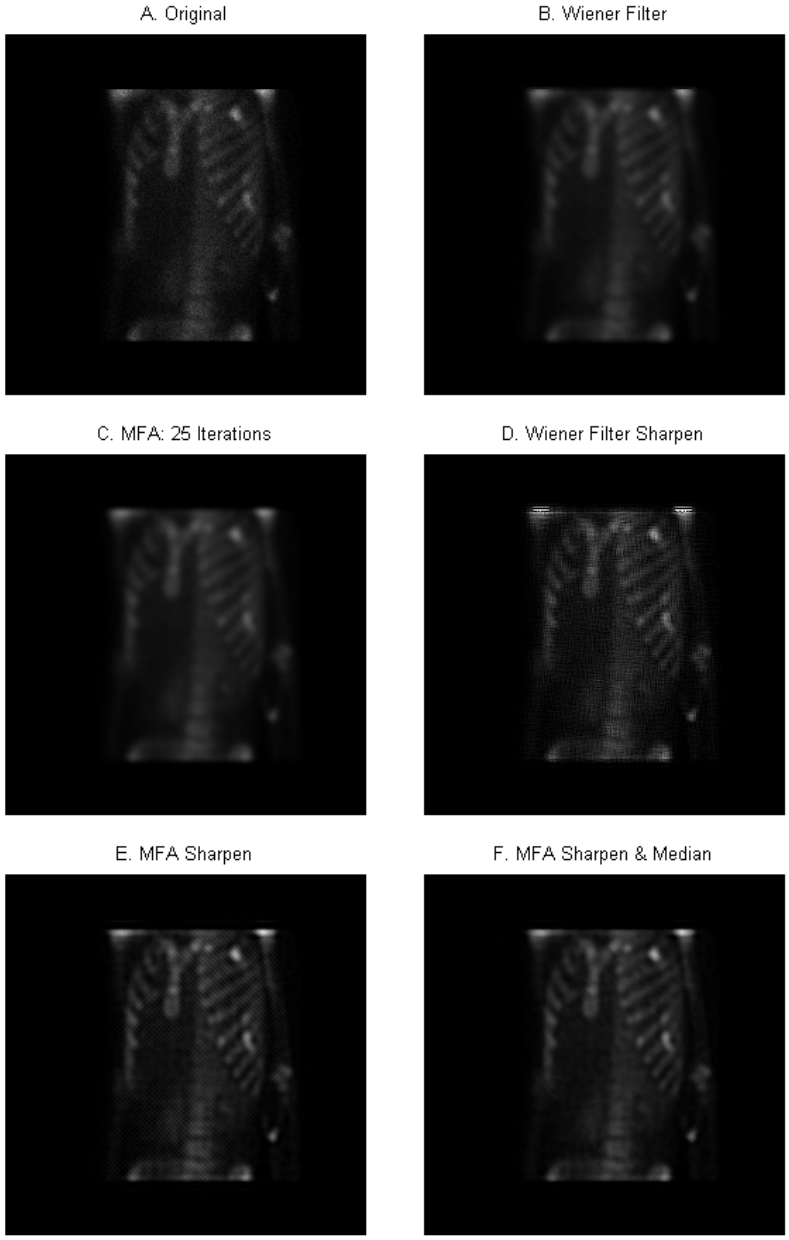

Figure 6.12: Results for LAO002. A:original bone scan, B: Wiener filter result, C: MFA result after 25 iterations, D: Wiener filter result sharpened, E: MFA result sharpened, F: MFA result sharpened and median filtered.

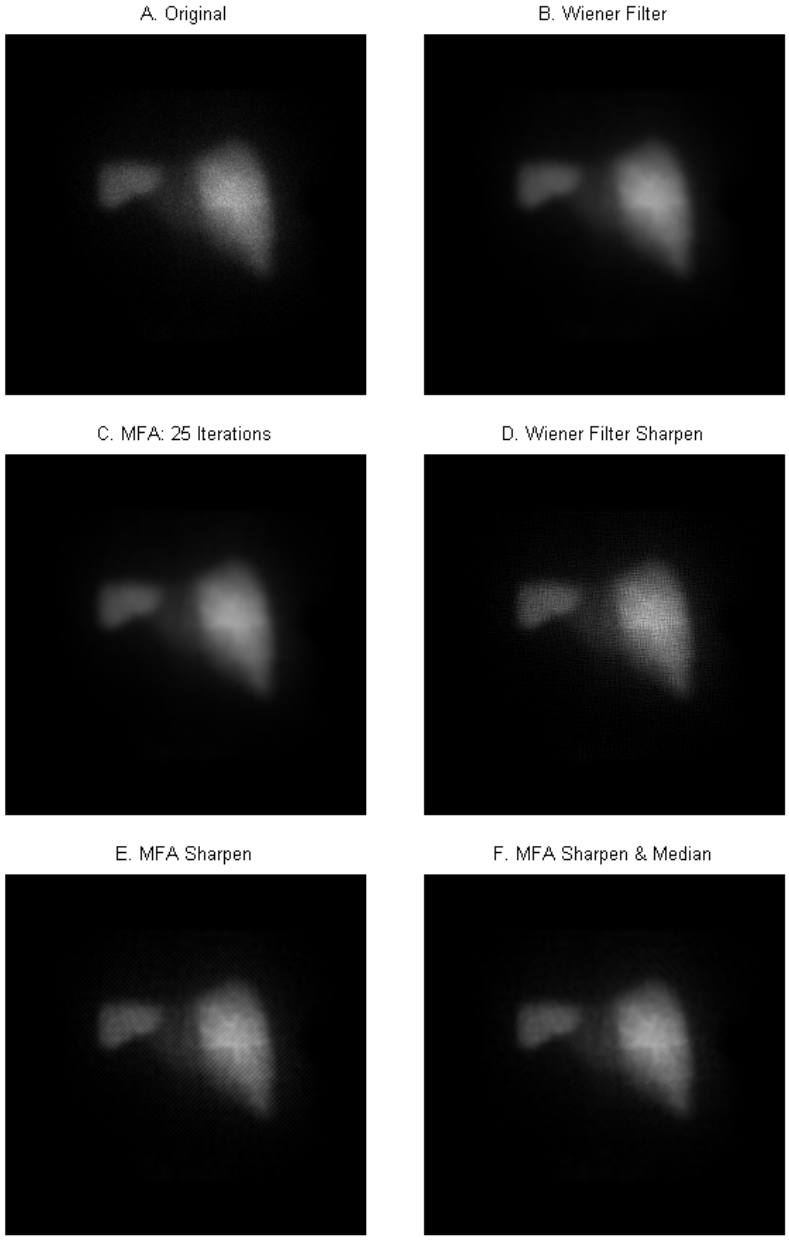

Figure 6.13: Results for POST001. A:original liver-spleen scan, B: Wiener filter result, C: MFA result after 25 iterations, D: Wiener filter result sharpened, E: MFA result sharpened, F: MFA result sharpened and median filtered.

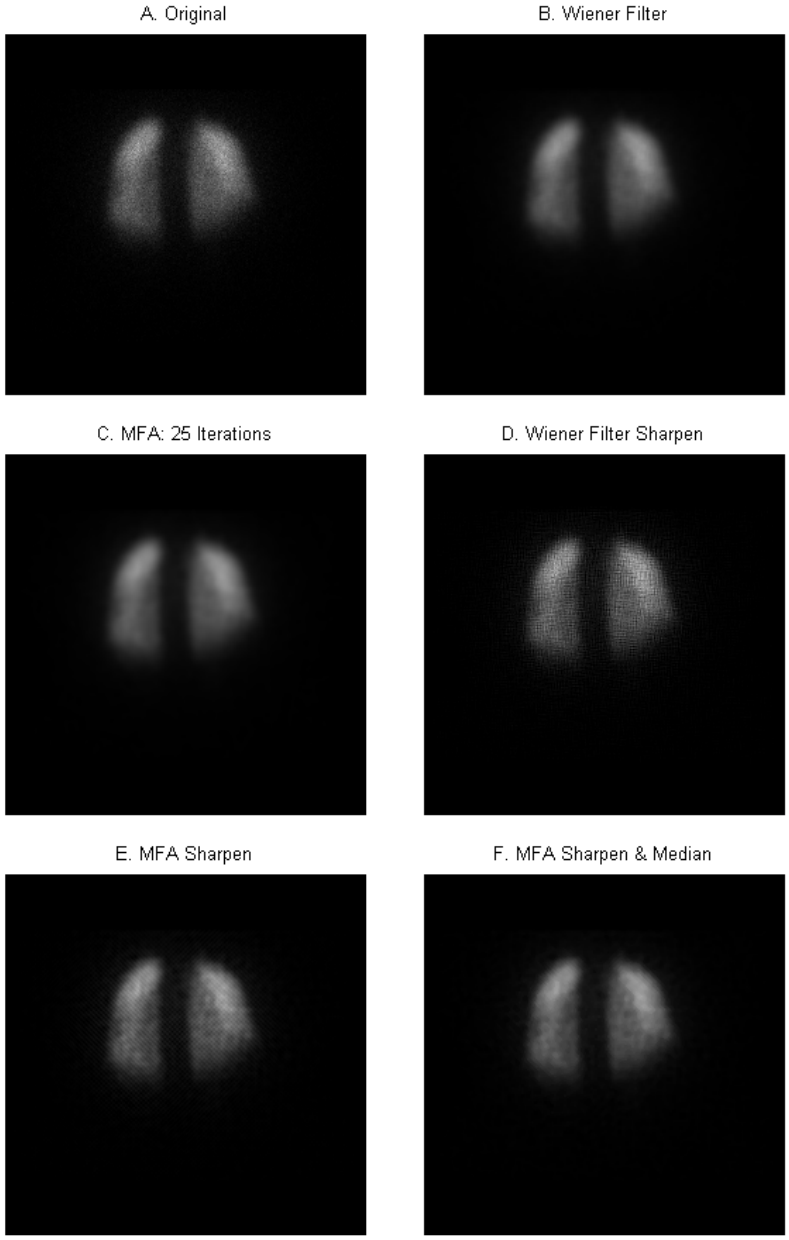

Figure 6.14: Results for POSTP002. A:original lung perfusion scan, B: Wiener filter result, C: MFA result after 25 iterations, D: Wiener filter result sharpened, E: MFA result sharpened, F: MFA result sharpened and median filtered.

Chapter 7

Conclusion

NM images can be difficult to diagnose, particularly where steep intensity gradients occur in the images. MFA, while providing intra-region blurring alone, does not visually highlight the edges, and for this reason image enhancement of planar NM images is achieved by implementing a noise-sensitive sharpening filter as a post-MFA processing technique. The result is a clearer and sharper image with more apparent viewable detail that may improve diagnosis. Applying, optimally, the same sharpening filter to a Wiener restored image does not yield the same standard of image enhancement compared to that of the MFA-sharpened image, as assessed subjectively.

The collimator is a limiting factor in the spatial resolution and also in image reconstruction. It is the PSF that provides the spatial information required to implement MFA. Approximate Gaussian-distributed PSF radial symmetry, as well as PSF non-uniformity with source depth has been illustrated. The PSF depth variance precludes complete image reconstruction, but does allow for enhancement of a single *plane of interest* per specified PSF, requiring the software running MFA to provide an adjustable PSF. This also highlights the importance of image presentation for NM physicians. Furthermore the PSF is shown to display a regional linear trend.

The development of the image restoration algorithm was greatly aided by using simple digital phantoms with known properties despite the fact that these digital phantoms are not ideal representations of clinical NM images.

A disadvantage of MFA is that there are a number of parameters that are required for the algorithm to be successful. The use of digital phantoms and empirical techniques have been shown in this study to yield approximate optimal parameters and stopping criteria for successful restoration of both digital phantoms and clinical NM

images. Note that the difference between optimal and sub-optimal results appears to be negligible in this application of MFA. A further disadvantage is that MFA restoration yields vertical and horizontal *fabric-like* artifacts that become diagonal *fabric-like* artifacts after a sharpening filter is applied. These artifacts, possibly attributable to edge operator weaknesses, can be removed with minimal image quality loss by implementing a median filter.

It is possible that an MFA enhanced image may in fact introduce artifacts that may mislead diagnosis. On the other hand addition of detail that was not previously visible may require NM physicians to recalibrate how they assess their diagnosis. MFA may also be more effective and suitable for particular types of NM images. It is therefore concluded that a full appraisal of MFA for numerous NM images of different types be conducted with the aid of NM physicians and medical physicists before a clinical assessment of this technique can be made.

With current processing technology, the computational time required to run the MFA algorithm is no longer significant and thus MFA holds promise as a supplementary pre-filter tool for the enhancement of diagnostic NM images.

7.1 Suggested Future Work

The following items are recommended for future work and research on the viability and improvement of MFA applied to NM clinical images.

- It is highly recommended that an extensive appraisal of MFA for various types of NM images be conducted with the aid of NM physicians and medical physicists.
- It is recommended that further research be done in acquiring a more suitable edge operator specific to NM images or particular NM image types such as bone, thyroid etc. The research will need to examine how to implement the prior Hamiltonian and its partial derivative with different edge operators.
- This MFA implementation was programmed in MATLAB for rapid development. Further work is recommended to convert the code to a lower level programming language for computational efficiency.
- Although not examined in-depth, it may be possible to use the noise and prior Hamiltonians as enhancement indicators and ultimately as the stopping

criteria that is vital for MFA operation. It may also be possible to utilize FWHM resolution of bar phantoms to characterize MFA improvement.

- Possible experimentation with Broyden-Fletcher-Goldfarb-Shannon and conjugate gradient methods instead of gradient descent may yield superior results.

- NM images suffer from PSFs that are both shift and depth variant. This MFA algorithm can be adapted to use varying PSFs corresponding to source depth (for depth variance) and across a plane (to deal with shift variance). This would require using many point sources at different points above the collimator (effectively using a three dimensional grid of point sources) to ascertain the depth and plane distributions of PSFs. It is also recommended that a more careful and thorough investigation of the factors influencing the PSF be conducted, and the fitted curve in Figure 6.4 improved.

- Enhancing NM images with PSFs of different standard deviations (associated with different depths) should yield enhancement of *planes of interest*, and it should be investigated how effectively the planes can be separated to reconstruct a three dimensional version of the planar NM image. Although there are numerous ways to accomplish this, it is highly recommended that a "movie" of restoration be used to verify how effectively *planes of interest* can be focused. Each frame in the "movie" will be an optimally restored image but restored with a consecutively changing PSF. This PSF may be attained from a graph or equation such as that shown in Figure 6.4.

- This MFA algorithm uses the initial estimate of noise for all the MFA iterations. It is believed that iteratively updating the estimate of decreasing noise as MFA runs could provide superior results. A flood source will only provide the initial estimate of noise, so an algorithm such as quadtree noise determination should be investigated in more depth. Other techniques developed for different applications such as noise evaluation in astronomical images [10] should be investigated for use in NM images.

Appendix A

MFA Code

Mean Field Annealing Algorithm

The following code implements the Mean Field Annealing (MFA) algorithm and it also illustrates the empirical methods used to determine the optimum parameters required in MFA for digital phantoms. Some of the code has been modified from *Adaptations of the MFA algorithm for the enhancement of Infrared Thermal Images* by Lindy Finn [5].

Contents

- Load the scene
- Simulated image acquisition
- Determine noise content
- Call ANVD function
- Restore using Wiener Filter
- Initialisations
- Parameter selection
- Reinitialisations
- MFA primary loop
- Gradient Descent loop
- Call the Noise Hamiltonian function
- Call the Prior Hamiltonian function
- Gradient Descent calculation
- Print results to screen.
- Function: Noise Variance Determination (ANVD)

- Function: Noise Hamiltonian Determination
- Noise Hamiltonian
- Derivation of Noise Hamiltonian partial derivative
- Function: Prior Hamiltonian Determination
- Derivation of Prior Hamiltonian
- Derivation of Prior Hamiltonian partial derivative

Load the scene

Load the ideal image referred to as the scene, this is the image that will be used to create the digital phantom.

```
clear;
I=imread('phanB.bmp');
I=im2double(I);
figure(1), imshow(I);
title('Original Image');
```

Simulated image acquisition

The following simulates the image acquisition process, adding blur and noise.

```
V=0.035; % Typical variance of the noise.
hsigma=2; % Variance of Guassian distribution associated with the blur.
hsize=5; % Size of PSF.
h=fspecial ('gaussian',hsize ,hsigma) ; % PSF.
hrev=fliplr(flipud(h)); % Reverse matrix of PSF.
I_blur=conv2(I,h,'same'); % Add blur.
I_blur_noise=imnoise(I_blur, 'gaussian', 0,V); % Add noise.
[RMSE0,PSNR0]=CalcError(I,I_blur_noise,h); % Calculate RMSE & PSNR.
figure(2), imshow(I_blur_noise);
title(['I blur noise RMSE: ',num2str(RMSE0),' PSNR: ',num2str(PSNR0)]);
```

Determine noise content

Restore image using Automatic Quadtree Variance Detection (ANVD)

Call ANVD function

```
var_approx=ANVD(I_blur_noise);  % Approximate variance.
```

Restore using Wiener Filter

```
[I_wiener]=wiener2(I_blur_noise,[5 5],var_approx); % Restore using Wiener.
[RMSE1,PSNR1]=CalcError(I,I_wiener,h);             % RMSE of Wiener for comparison.

figure(3), imshow(I_wiener);
title(['I wiener RMSE: ',num2str(RMSE1),' PSNR: ',num2str(PSNR1)]);
```

Initialisations

fk is the running approximation to the original image In this case our first approximation is the realimage.

```
fk=I_blur_noise;               % Make I_blur_noise the first approximation.
var_approx=0.0035;             % The variance is known.
g=I_blur_noise;                % g is the recorded image.
[RMSE,PSNR]=CalcError(I,fk,h); % I=Original scene. fk=current image.
```

Parameter selection

The following five loops run through different combinations of parameters to find optimum parameters for MFA image restoration.

```
MAIN_c=0;
% Optimals used for NM
for beta_coeff=[2 10 50 100]                % 100
for T_start=[sqrt(var_approx)*10 0.5 1 2]   % sqrt(var_approx)*10
for grad_decent_iters=[10 20 50]            % 20
for relax_ratio=[0.1 0.4 1 1.5 2 2.5 10 15] % 2.5
for alpha_method=[1 2]                      % 1
```

Reinitialisations

Reinitialise the MFA settings for each parameter loop.

```
fk=I_blur_noise;                % Reinitialise fk as the running approximation.
[RMSE,PSNR]=CalcError(I,fk,h); % I=Original scene. fk=current image.
MAIN_c=MAIN_c+1;
T=T_start;
MFA_iter=0;
Tend=T/60;
RMSE_prev=RMSE;
H_total=0;
Total_count=0;
```

MFA primary loop

Main MFA while loop.

```
while RMSE <= RMSE_prev & T>Tend

    MFA_iter=MFA_iter+1;
    RMSE_prev=RMSE;
    beta=sqrt(var_approx)*beta_coeff;
```

Gradient Descent loop

```
  % Begin Gradient Descent loop.


     for grad_descent_iter=1:grad_descent_iters;
         Total_count=Total_count+1;
```

Call the Noise Hamiltonian function

```
     % Determine Noise Hamiltonian and its partial derivative.


        [H_noise,pdH_noise]=NHamil(fk,g,h,hrev,V);
```

Call the Prior Hamiltonian function

```
     % Determine Prior Hamiltonian and its partial derivative.


        [H_prior,pdH_prior,Hp_num2]=PHamil(fk,T,'quadratic');

        tempH=H_total;
```

```
H_total=H_noise +beta*H_prior;      % Total Hamiltonian.
pdH_total=pdH_noise+beta*pdH_prior; % and its partial derivative.

Hchange=H_total-tempH;
if Hchange >0
    gamma=0.5;
else
    gamma=1;
end

if alpha_method==1                  % First alpha method.

 deltaf=pdH_total;
 if deltaf==inf
        MLF=1;
        'MLF inf'
    elseif deltaf==0
        MLF=1;
        'MLF 0'
    elseif deltaf==-inf
        MLF=-1;
        'MLF -inf'
    else
        MLF=sqrt(norm(deltaf));
    end
    alpha=0.05*(sqrt(var_approx*T)/MLF)*relax_ratio;
end

if alpha_method==2                  % Second alpha method.

    if pdH_total==inf
        MLF=1;
        'MLF inf'
    elseif pdH_total==0
        MLF=1;
        'MLF 0'
    elseif pdH_total==-inf
        MLF=-1;
        'MLF -inf'
    else
        MLF=sqrt(mean2(pdH_total.^2));
    end
    alpha=0.05*gamma*(sqrt(var_approx*T)/MLF)*relax_ratio;

end
```

Gradient Descent calculation

```
fkNew=fk-alpha*pdH_total;
```

```
        fk=fkNew;

        [RMSE,PSNR]=CalcError(I,fk,h);
        % Write results screen.
        fprintf('M_c=%f T_c=%f H_T=%f RMSE=%f PSNR=%f beta=%f T_s=%f'...
        'grad_it=%f relax=%f alp_m=%f  MFA_it=%f alp=%f\n '  ,MAIN_c,...
        Total_count,H_total,RMSE, PSNR, beta_coeff,T_start,...
        grad_descent_iters, relax_ratio,alpha_method, MFA_iter, alpha);
        Totalresults(Total_count,:)=[Total_count T RMSE PSNR H_total];

    end  % Ends gradient descent main loop

    [RMSE,PSNR]=CalcError(I,fk,h);
    T=0.95*T;  % Decrease the temperature.

    % Document results.
    results1(MAIN_c,:)=[MAIN_c beta_coeff  T_start grad_descent_iters...
    relax_ratio alpha_method MFA_iter RMSE PSNR T];

end  % ends MFA while loop

results2(MAIN_c,:)=[MAIN_c beta_coeff  T_start grad_descent_iters relax_ratio...
    alpha_method MFA_iter RMSE PSNR];

end % alpha_method
end % relax_ratio
end % grad_descent_iters
end % start_temp
end % beta_coeff
```

Print results to screen.

```
[RMSEf,PSNRf]=CalcError(I,fk,h);
figure(20), imshow(fk);
title(['I after MFA RMSE: ',num2str(RMSEf),' PSNR: ',num2str(PSNRf)]);

figure(22), imshow(abs(fk-I_blur_noise));
title(['I after MFA RMSE: ',num2str(RMSEf),' PSNR: ',num2str(PSNRf)]);
```

Function: Noise Variance Determination

This function uses quadtree decomposition and optimisation to calculate the approximate noise variance of an image.

```
function [NoiseVarGuess]= ANVD(I_real,Thresh_Const);
```

```
% M=[cellstr('General Count')  cellstr('Thresh Const')
% cellstr('Determined_Var')  cellstr('No. Blocks')]

I_real=im2double(I_real);

General_count=0;
Average_Var=0.0053; % First guess.
Average_Var_Prev=0.0022; % Just to get things going
General_count=0;
while (abs(Average_Var-Average_Var_Prev) > 0.0005) & (General_count <50)

Average_Var_Prev=Average_Var;
General_count=General_count+1;

% 94 percent of pixel intensity variations should be encompassed
% by this value of threshhold
Threshhold=sqrt(Average_Var)*Thresh_Const;
S=qtdecomp(I_real,Threshhold,1);

Block=0;
Average_Var=0;

for DIM=[256 128 64 32 16 8 4 2] % for loop 1
[Vals,R,C]=qtgetblk(I_real,S,DIM);

for temp=1:size(R)  % for loop 2
    I_little_quad=imcrop(I_real,[C(temp) R(temp) DIM DIM]);

    [x_S y_S]=size(I_little_quad);
    sum=0;
    counter=0;
    % the following two "for" loops calculate the the sum of pixel
    % intensities for average calculations.
    for x=1 :x_S
        for y=1:y_S
        sum=sum+I_little_quad(x, y);
        counter=counter+1;
        end;
    end;
    % Calculate average of pixel intensities and creates
    % an image of averages.
    Ave=sum/counter;
    Quad_Image_noise(R(temp):R(temp)+DIM-1,C(temp):C(temp)+DIM-1)=Ave;

    % This draws the quads with black lines.
    Quad_Image_noise(R(temp):R(temp)+DIM,C(temp))=0;
    Quad_Image_noise(R(temp)+DIM,C(temp):C(temp)+DIM)=0;
    Quad_Image_noise(R(temp),C(temp):C(temp)+DIM)=0;
    Quad_Image_noise(R(temp):R(temp)+DIM,C(temp)+DIM)=0;
```

```
    % The following code is used to calculate the variance in each quad
    sum=0;
    counter=0;
    for x=1 :x_S
        for y=1:y_S
        sum=sum+(I_little_quad(x, y)-Ave)^2;
         counter=counter+1;
        end;
     end;
     Var=sum/(counter-1);
     % Once the variance has been calculated, it only contributes to the
     % average variace if its average falls between 0.2 and 0.8, this is
     % done to avoid errors caused by pixel intensity edges, i.e. 0 and 1
     if (Ave> 0.2) & (Ave< 0.8)
         Block=Block+1;
        Average_Var=Average_Var+Var;
    end
end % ends for loop 2

end % ends for loop 1
Average_Var=Average_Var/Block;
fprintf('G_c1=%f Thresh_Const=%f Average_Var=%f No. Blocks=%f \n' ,...
    General_count, Thresh_Const,Average_Var ,Block);

% The next guess is half way between the previous guessed variance and the
% determined variance using quadrature decomposition.
Average_Var=(Average_Var+Average_Var_Prev)/2; %Next guess.

end % ends while loop

NoiseVarGuess=Average_Var;
```

Function: Noise Hamiltonian Determination (ANVD)

This function takes in the current restoration image, fk=g, f is the original image, the PSF (h) and the variance of the noise V to determine the NOISE HAMILTONIAN and PARTIAL DERIVATIVE of the NOISE HAMILTONIAN.

```
function [H_noise, pdH_noise]= NHamil(g,f,h,hrev,V);

[M1,M2]=size(f) ;
Hn_num1=conv2(f,h,'same') ;
Hn_num2=zeros(M1,M2);      % Create zero matrix same size as fk.
Hn_num2=g-Hn_num1;
```

Noise Hamiltonian

```
Hn_num3=Hn_num2.^2;
H_noise=sum(Hn_num3(:))/(2*V);
```

Derivation of Noise Hamiltonian partial derivative

```
pdH_noise=conv2(Hn_num2,hrev,'same')/V;
```

Function: Prior Hamiltonian Determination

This function takes in the current restoration image,fk, the temperature, T and the method with which to determine the PRIOR HAMILTONIAN and PARTIAL DERIVATIVE of the PRIOR HAMILTONIAN.

```
function [H_prior, pdH_prior,Hp_num2]= PHamil(fk,T,Method);
% Note, the beta term has NOT been included in this function and must be
% included in the main program

Hp_den1=T^2;  % the denominator term.

switch lower(Method)
   case 'linneighbor'

       Edgematrix=zeros(size(fk,1),size(fk,2));

            for x=11:1:size(fk,1)-11
                for y=11:1:size(fk,2)-11
                     for xi=1:1:6
                          for yi=1:1:6
                               Edgematrix(x,y)=Edgematrix(x,y)+(fk(x,y)-...
                                   fk(x+3-xi,y+3-yi))^2;
                           end
                     end
                end
            end

       Hp_num2=exp(-(Edgematrix)/(2*Hp_den1));

    case 'quadratic'
```

Derivation of Prior Hamiltonian

```
     qxx=1/sqrt(6)*[0 0 0; 1 -2 1; 0 0 0];
qyy=1/sqrt(6)*[0 1 0; 0 -2 0; 0 1 0];
qxy=1/2*[-1 0 1; 0 0 0; 1 0 -1] ;
Edge1=conv2(fk,qxx,'same'); Edge2=conv2(fk,qyy,'same');
        Edge3=conv2(fk,qxy,'same');
Edgematrix=Edge1.^2+Edge2.^2+2*Edge3.^2;
        Hp_num2=exp(-(Edgematrix)/(2*Hp_den1));
        Hp_num3=sum(Hp_num2(:));
        H_prior=-(1/(sqrt(pi*2)*T))*Hp_num3 ;  % PRIOR note this term is negative.
```

Derivation of Prior Hamiltonian partial derivative

```
        qxxrev=fliplr(flipud(qxx)); qyyrev=fliplr(flipud(qyy) ) ;
        qxyrev=fliplr(flipud(qxy)) ;
        Hp_PD_num1=Hp_num2;
        Hp_PDxx=Edge1.*Hp_PD_num1 ;
        Hp_PDyy=Edge2.*Hp_PD_num1;
        Hp_PDxy=Edge3.*Hp_PD_num1;
        pdHp2=conv2(Hp_PDxx,qxxrev,'same')+conv2(Hp_PDyy,qyyrev,'same')+...
            conv2(Hp_PDxy,qxyrev,'same') ;
        pdH_prior=1/ (sqrt(pi*2) *T*Hp_den1) *pdHp2;   % PD of PRIOR
        % Note the absence of the Beta term and that this term is positive.

    case 'sobel'
        hy = fspecial('sobel');
        hx = hy';
        Iy = imfilter(double(I_wiener), hy, 'replicate');
        Ix = imfilter(double(I_wiener), hx, 'replicate');
        Edgematrix = sqrt(Ix.^2 + Iy.^2);
        Hp_num2=exp(-(Edgematrix)/(2*Hp_den1));


otherwise
      disp('ERROR: Unknown edge method.')
end
```

Appendix B

MFA restoration program

Figure B.1 shows the program used to determine the results for this report. The program allows the user to scroll using a sliderbar through a set of consecutive MFA iterated images. Advanced versions of this software would include automatic image sharpening filter utilities, median filters and other suitable post-processing techniques. In addition the software should allow the user to enhance an image using multiple PSFs. The user can then scroll through a "movie" of optimal image restoration sets at different PSFs to possibly view detail at different depths, i.e. *planes of interest*. This particular program was written in MATLAB's GUIDE GUI utility.

Figure B.1: Screen shot of a Graphical User Interface used to produce a movie of consecutive iterations.

Appendix C

Enlarged Results

This appendix displays enlarged original bone NM clinical images with their respective MFA enhancement results. Note that in a printed form these results are not as visually effective as in digital form (see Appendix D for electronic version of the results).

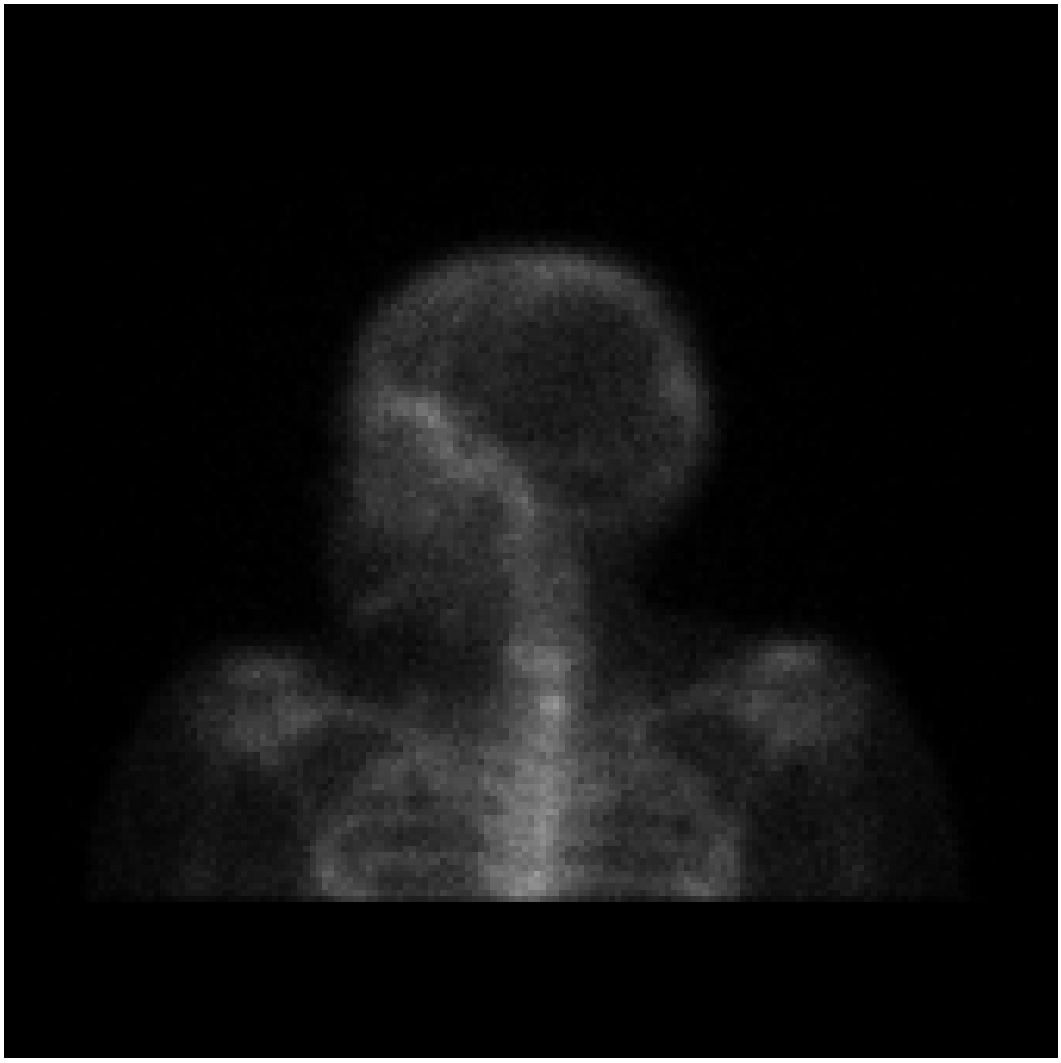

Figure C.1: LLATS: Enlarged original image.

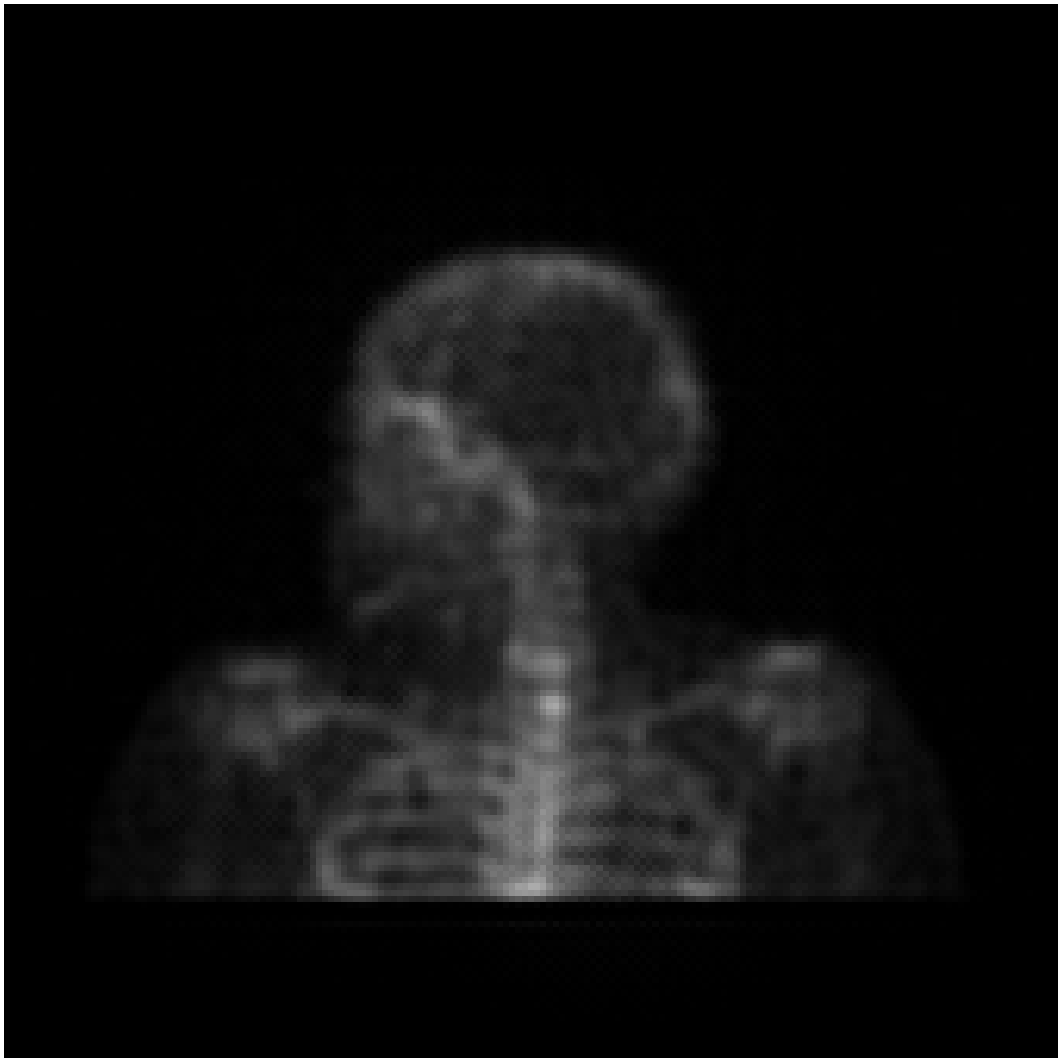

Figure C.2: LLATS: Enlarged result after 25 MFA iterations and sharpened.

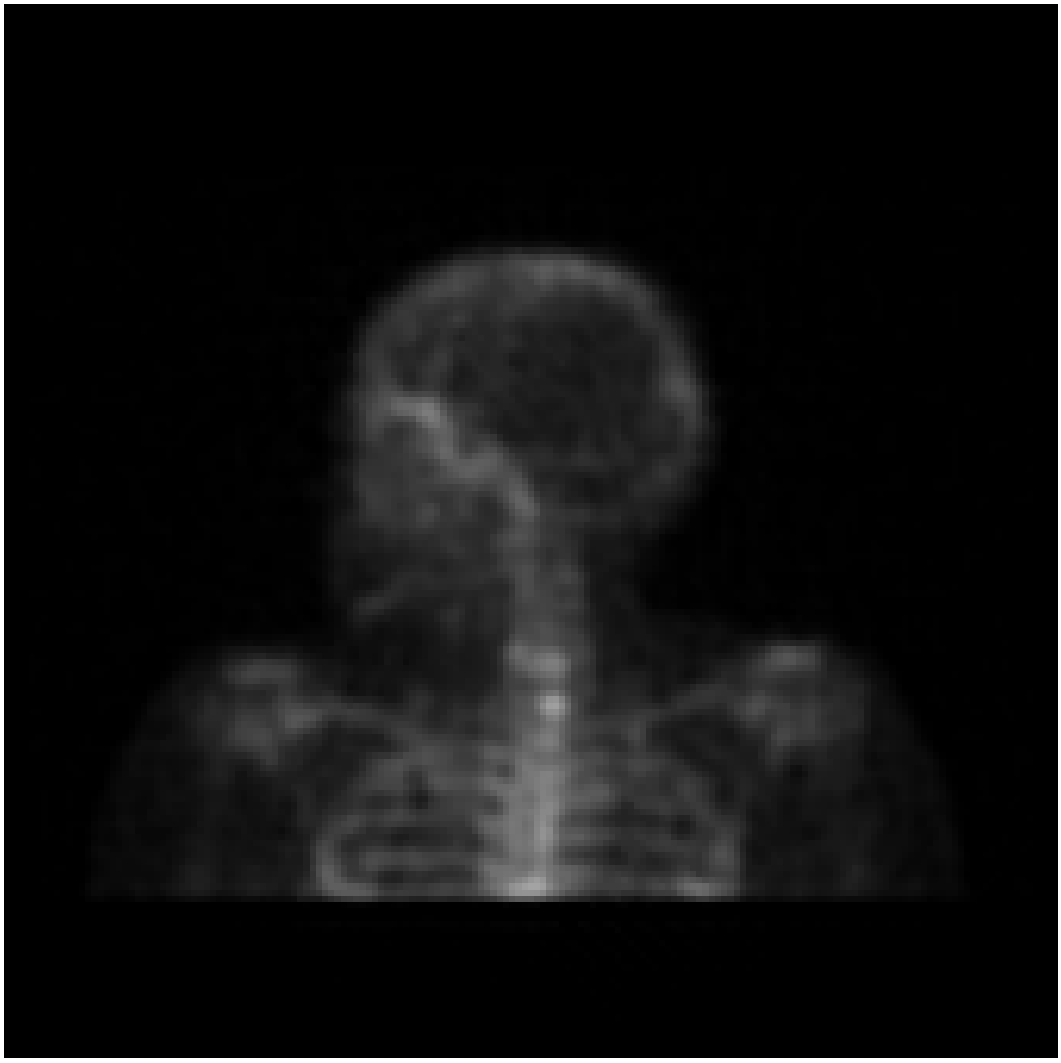

Figure C.3: LLATS: Enlarged result further Median filtered.

Figure C.4: LAO001: Enlarged original image.

Figure C.5: LAO001: Enlarged result after 25 MFA iterations and sharpened.

Figure C.6: LAO001: Enlarged result further Median filtered.

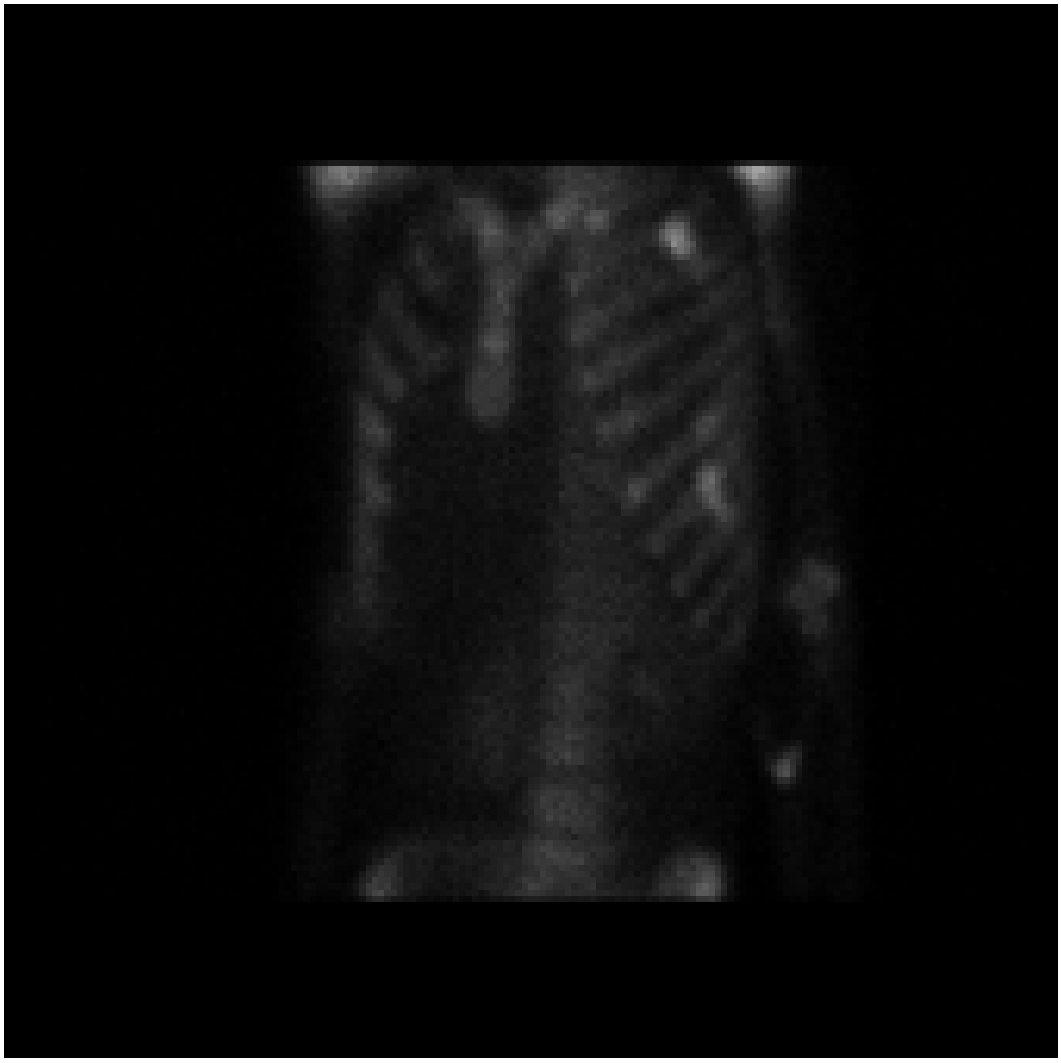

Figure C.7: LAO002: Enlarged original image.

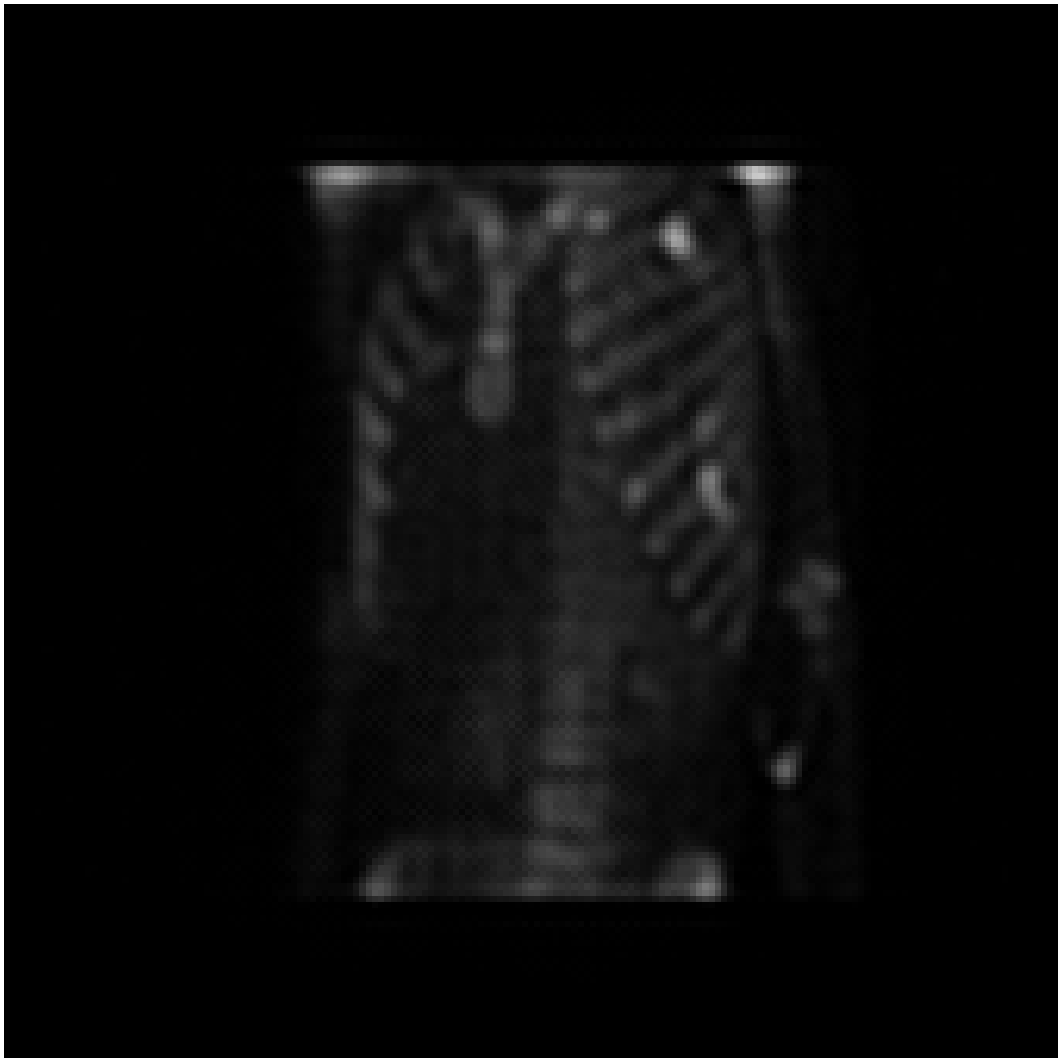

Figure C.8: LAO002: Enlarged result after 25 MFA iterations and sharpened.

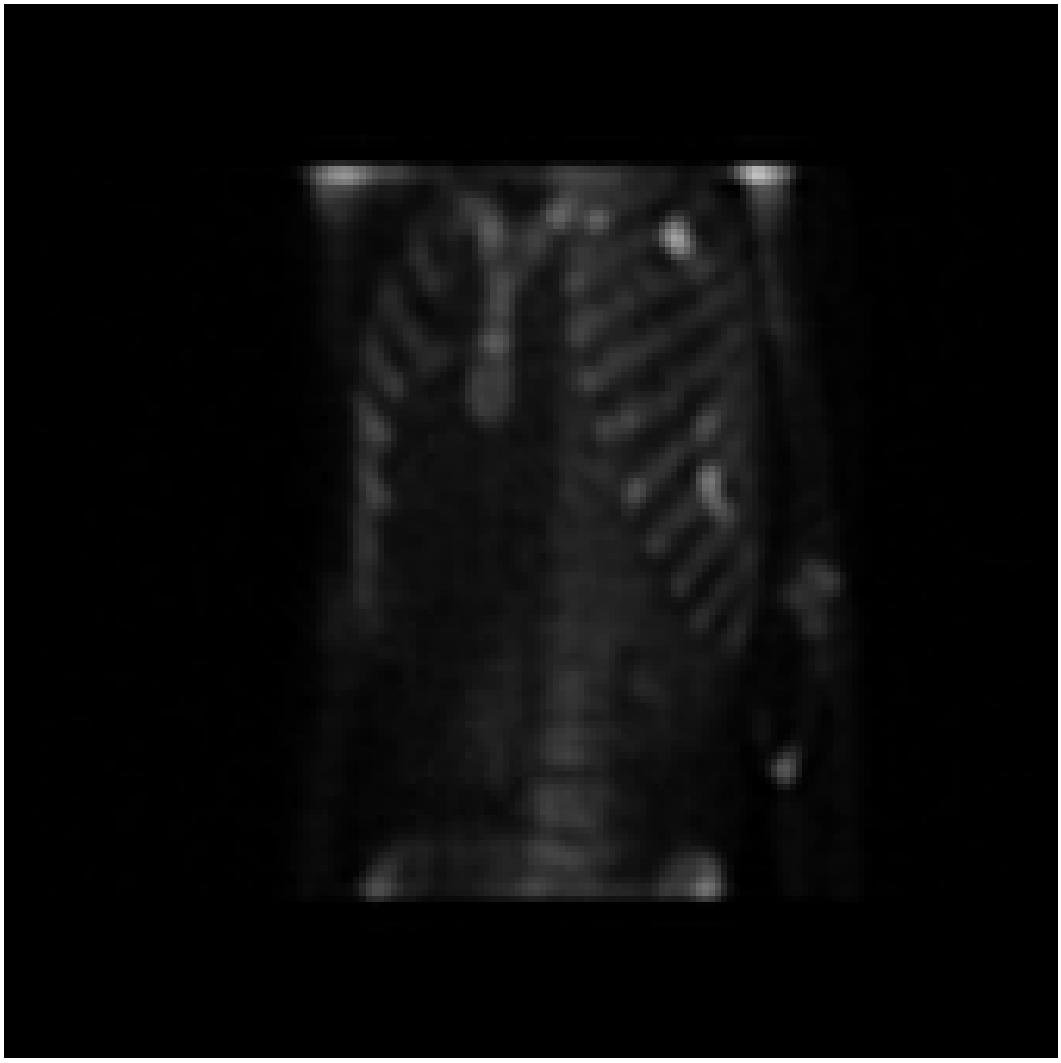

Figure C.9: LAO002: Enlarged result further Median filtered.

Appendix D

Electronic Copy of Images and Source Code

See the inside of the back cover for a cd containing an electronic copy of images and source code.

References

[1] O. Glasser, "The Science of Radiology," *Springfield, IL Charles C Thomas*, 1934.

[2] D. L. Falk D. M. Rubin T. Marwala, "Enhancement of Noisy Planar Nuclear Medicine Images using Mean Field Annealing," *World Congress of Medical Physics and Biomedical Engineering*, vol. 14, pp. 2297–2300, 2006.

[3] S. R. Cherry J. A. Sorenson M. E. Phelps, *Physics in Nuclear Medicine*, Saunders, third edition, 2003.

[4] S. Akber H. Greenspan, C. H. Anderson, "Image Enhancement by Nonlinear Extrapolation in Frequency Space," *IEEE Transactions on Image Processing*, vol. 9, no. 6, pp. 1035–1048, 1994.

[5] L. K. Finn, "Adaptations of the MFA algorithm for the enhancement of Infrared Thermal Images," *MSc Dissertation, University of the Witwatersrand*, p. 6, 2003.

[6] W. Snyder Y. Han G. Bilbro R. Whitaker S. Pizer, "Image Relaxation: Restoration and Feature Extraction," *IEEE Transactions on Pattern Analysis and Machine Intelligence*, vol. 17, no. 6, 1995.

[7] G. L. Bilbro W. E. Snyder S. J. Garnier J. W. Gault, "Mean Field Annealing: a formalism for constructing GNC-like algorithms," *IEEE Trans. Neural Networks*, vol. 3(1), pp. 131–138, 1992.

[8] L. P. Clarke W. Qian, "Wavelet-Based Neural Network with Fuzzy-Logic Adaptivity for Nuclear Image Restoration," *Proceedings of the IEEE*, vol. 84, pp. 1458–1473, 1996.

[9] D. Geman, "Random fields and inverse problems in imaging," *Lecture Notes in Mathematics, Springer-Verlag, Berlin-Heideberg-New York*, vol. 1427, pp. 117–193, 1991.

[10] J. Starck F. Murtagh, "Automatic Noise Estimation from the Multiresolution Support," *Publications of the Astronomical Society of the Pacific*, vol. 110, pp. 193–199, February 1998.

[11] S. I. Olsen, "Estimation of noise in images: an evaluation," *CVGIP: Graphical Models and Image Processing*, vol. 55, no. 4, pp. 319–323, 1993.

[12] B. R. Hunt H. C. Andrews, "Digital Image Restoration," *Prentice-Hall, Englewood Cliffs, NJ*, 1977.

[13] W. E. Snyder C. X. Wang, "MAP Transmission Image Reconstruction via Mean Field Annealing for Segmented Attenuation Correction of PET Imaging," *IEEE-EMBC and CMBEC*, pp. 517–518, 1997.

[14] W. E. Snyder H. Qi R. L. Elliott J. F. Head C. X. Wang, "Increasing the Effective Resolution of Thermal Infrared Images," *Engineering in Medicine and Biology Magazine, IEEE*, vol. 19(3), pp. 63–70, 2000.

[15] D. Chandler, *Intoduction to Modern Statistical Mechanics*, Oxford University Press, first edition, 1987.

[16] P. Perez, "Markov Random Fields and Images," *CWI Quarterly*, vol. 11(4), pp. 413–437, 1998.

[17] A. C. Bovik S. T. Acton, "Anisotropic edge detection using Mean Field Annealing," *IEEE International Conference on Acoustics,Speech, and Signal Processing*, vol. 2, pp. 393–396, 1992.

[18] S. T. Acton, "Diffusion-Based Edge Detectors," *Handbook of Image and Video Processing*, p. 433, 1993.

[19] L. Small C. Wang W. Snyder R. Williams, "Edge Detection in Gated Cardiac Nuclear Medicine Images," *Seventh Annual IEEE Symposium on Computer-Based Medical Systems,IEEE Transactions on Image Processing*, pp. 28–33, 1994.

[20] G. L. Bilbro R. Mann T. K. Miller W.E. Snyder M. White, "Optimization by Mean Field Annealing," *Advances in Neural Network Information Processing Systems (D.S. Touretzky, ed.)*, pp. 91–98, 1989.

[21] F. Girosi D. Geiger, "Parrallel and deterministic algorithms from MRF's: Surface reconstruction," *IEEE Trans. Patt. Anal. Machine Intell.*, vol. 13(5), pp. 401–412, 1991.

[22] L. Ingber, "Simulated Annealing: practice versus theory," *Mathl. Comput. Modelling*, vol. 18(11), pp. 29–57, 1993.

[23] M. N. Rosenbluth A. H. Teller E. Teller N. Metropolis, A. E. Rosenbluth, "Equation of state calculations by fast computing machines," *The Journal of Chemical Physics*, vol. 21(6), pp. 1087–1092, 1953.

[24] S. Kirkpatrick C. D. Gelatt M. P. Vecchi, "Optimization by Simulated Annealing," *Science*, vol. 220(4598), pp. 671–680, 1983.

[25] L. Ingber, "Genetic algorithms and Very Fast Simulated Reannealing: A comparison," *Mathematical and Computer Modelling*, vol. 16(11), pp. 87–100, 1992.

[26] L. Ingber, "Adaptive Simulated Annealing (ASA): Lessons learned," *special issue of the Polish Journal Control and Cybernetics on Simulated Annealing Applied to Combinatorial Optimization*, vol. 25(1), pp. 33–54, 1996.

[27] Computational Science Education Project, "Mathematical Optimization," *http://www.phy.ornl.gov/csep/CSEP/MO/NODE28A.html*, Last accessed 11 February 2007.

[28] W. K. Hastings, "Monte Carlo Sampling Methods Using Markov Chains and Their Applications," *Biometrika*, vol. 57(1), pp. 97–109, 1970.

[29] S. Chib E. Greenburg, "Understanding the Metropolis-Hastings Algorithm," *American Statistician*, vol. 49(4), pp. 327–335, 1995.

[30] H. P. Hiriyannaiah G. L. Bilbro W. E. Snyder R. C. Mann, "Restoration of piecewise-constant images by Mean-Field Annealing," *J. Opt. Soc. Am. A.*, vol. 6(12), pp. 1901–1912, 1989.

[31] J. Zhang, "The Mean Field Theory in EM Procedures for Blind Markov Random Field Image Restoration," *IEEE Trans. Image Processing*, vol. 2(1), pp. 27–40, 1993.

[32] J. Hanauer J. Zhang, "The Mean Field Theory for image motion estimation," *Proc. IEEE Int. Conf. Acoust. Speech., Signal Processing*, pp. V197–V200, 1993.

[33] W. Snyder A. Logenthiran P. Santago K. Link G. Bilbro S. Rajala, "Segmentation of magnetic resonance images using Mean Field Annealing," *Proceedings of Int. Conf. on Information Processing in Medical Imaging*, pp. 218–226, 1991.

[34] R. Chellappa J. Zerubia, "Mean Field Approximation using compound Gauss-Markov field models for edge detection and image estimation," *IEEE Trans. Neural Network*, vol. 4(4), pp. 703–709, 1993.

[35] R. Horaud L. Herault, "Finger-ground discrimation: A combinational optimization approach," *IEEE Trans. Patt. Anal. Machine Intell.,*, vol. 15(9), pp. 899–914, 1993.

[36] C. A. Bouman, "Markov Random Fields and Stochastic Image Models," *Tutorial presented at IEEE International Conference on Image Processing, Washington*, October 1995.

[37] T. Bayes, "An essay towards solving a Problem in the Doctrine of Chances," *Philosophical Transactions of the Royal Society of London*, vol. 53, pp. 370–418, 1763.

[38] C.P. Robert G. Casella, *Monte Carlo Statistical Methods*, New York: Springer-Verlag, second edition, 2004.

[39] H. Qi W. E. Snyder G. L. Bilbro, "Using Mean Field Annealing to Solve Anisotropic Diffusion Problems," *International Conference on Image Processing*, vol. 3, pp. 352, 1997.

[40] W. E. Snyder Y. Han, "New Apllications of Mean Field Annealing to the Restoration of Medical Images," *Annual International Conference of the IEEE Engineering in Medicine and Biology Society*, vol. 13(1), pp. 97–98, 1991.

[41] C. Wang W. E. Snyder, "Improving the Resolution of Infrared Images of the breast," *18th Annual International Conference of the IEEE Engineering in Medicine and Biology Society*, vol. 5, pp. 2087–2088, 1996.

[42] R. Chellappa A. Rangarajan, "Markov Random Field Models in image processing," *The Handbook of Brain Theory and Neural Networks, MIT Press*, 1995.

[43] D. Geman S. Geman, "Stochastic relaxation, Gibbs distributions and Bayesian restoration of images," *IEEE Trans. Patt. Anal. Machine Intel.*, vol. 6(6), pp. 721–741, 1984.

[44] H. Goldstein, *Classical Mechanics*, p. 16, Addison-Wesley, second edition, 1980.

[45] J. Besag, "On the statistical analysis of Dirty pictures," *J. R. Statist. Soc. B*, vol. 48(3), pp. 259–302, 1986.

[46] A. Zisserman A. Blake, "Visual Reconstruction," *MIT Press, Cambridge MA*, 1987.

[47] D. McClure S. Geman, "Bayesian image analysis: an application to Single Photon Emission Tomography," *Proc Statistical Comp Sect,Am Statistical Association, Washington DC*, pp. 12–18, 1985.

[48] R. Leahy T. Hebert, "A generalized EM algorithm for 3D Bayesian reconstruction from Poison data using Gibbs priors," *IEEE Trans Med Imaging, June*, 1989.

[49] Y. Han D. M. Herrington W. E. Snyder, "Quantitive Angiography Using Mean Field Annealing," *Bowman Gray School of Medicine, Winston-Salem, NC*, 1992.

[50] A. D. Marshall, "Vision Systems: Gradient Based Methods," *http://homepages.inf.ed.ac.uk/rbf/CVonline/marshall*, Last accessed 11 February 2007.

[51] R. Boyle R. Thomas, "Computer Vision: A First Course," *Blackwell Scientific Publications*, pp. 50–51, 1988.

[52] R. Gonzalez R. Woods, "Digital Image Processing," *Addison Wesley*, pp. 414–428, 1992.

[53] M. Brady B. K. P. Horn, "Rotationally Symmetric Operators for Surface Interpolation," *Massachusetts Institute of Technology Artificial Intelligence Laboratory*, November 1981.

[54] R. Fisher S. Perkin A. Walker, "Spatial Filters," *http://homepages.inf.ed.ac.uk/rbf/ HIPR2/ log.htm*, Last accessed 11 February 2007.

[55] J. Canny, "A Computational Approach to Edge Detection," *IEEE Transactions on Pattern Analysis and Machine Intelligence*, vol. 8, pp. 679–714, 1986.

[56] C. X. Wang, "Optimal Image Interpolation Using Optimal Method, PhD Dissertation, North Carolina State University," 1996.

[57] M. Avriel, *Nonlinear Programming: Analysis and Methods*, p. 88, Dover Publishing, 2003.

[58] C. G. Broyden, "The convergence of a class of double-rank minimization algorithms," *Journal of the Institute of Mathematics and Its Applications*, vol. 6, pp. 222–231, 1970.

[59] W. E. Snyder G. L. Bilbro, "Applying Mean Field Annealing to Image Noise Removal," *Journal of Neural Network Computing, Technology, Design, and Applications*, vol. Fall, pp. 5–16, 1990.

[60] A. C. Kak M. Slaney, "Principles of Computerized Tomographic Imaging," *New York: IEEE press*, 1998.

[61] A. K. Jain, *Fundamentals of Digital Image Processing, Englewood Cliffs, NJ*, p. 439, Prentice Hall, 1989.

[62] K. Sohn J. H. Kim, "Parameter Estimation of Mean Field Annealing Technique," *IEEE Proceedings of Southeastcon 1997*, pp. 215–219, April 1997.

[63] S.G. Chang Y. Bin M. Vetterli, "Adaptive wavelet thresholding for image denoising and compression," *IEEE Transactions on Image Processing*, vol. 9(9), pp. 1532–1546, 2000.